Master Thesis Report

Designing a bone fracture apparatus for surgical training applied on human cadaver

---

by

Wenhao Wang

Student Name	Wenhao Wang
Student Number	5166225
Supervisor	Dr.ir. Tim Horeman
Co-supervisor	Prof.dr. J. Dankelman
Assistant supervisor	Drs. Masie Rahimi
Faculty	Faculty of Mechanical, Maritime and Materials Engineering, Delft
Company	Amsterdam Skill Centre

TU Delft

***Abstract*—fracture simulation is crucial for understanding bone fractures and their underlying physiology and pathophysiology. To achieve this objective, a collaborative effort between the Amsterdam Skill Centre (ASC) and TU Delft (TUD) culminated in the development of an innovative fracture device. The ASC's surgical department furnished us with a set of requisites, which we meticulously classified into 12 pivotal design criteria, each associated with anticipated performance outcomes. The design approach revolved around two primary functions: fracture execution and specimen preparation. Brainstorming sessions are extensive and ultimately create an all-encompassing mind map full of actionable ideas which contributes to two conceptual designs and, combining criteria evaluation, ultimately identifying the most suitable one. The analysis focus on energy release system and stability during the impact. The materialization phase encompassed an array of metalworking processes, including chainsaw cutting, turning, milling, and drilling. AISI 304L stainless steel, S355+J structural steel, and AW-6082-T6 aluminum were used for manufacturing. Drop tests were conducted using simulation bone, homogeneous material, and reinforced material. Weight tests demonstrated the device's potential to create fractures with low impact energy and proved the stability of the constructed system. Further work is required to refine impact force estimation and cadaver specimen test. This study provides a comprehensive examination of a controllable fracture device, offering insights into its construction, potential improvements, and the exploration of a compact variant tailored for specific cadaveric regions.**

I. Introduction

Training using human cadaveric models has been essential to surgical education since "De Humani Corporis Fabrica Libri Septem" was published in 1543[1]. Today, cadaveric dissection has become common practice in medical education and training, offering medical students and healthcare professionals a valuable opportunity to learn about anatomy and physiology in a three-dimensional and realistic setting, as opposed to textbooks or virtual models. Especially for trauma surgery and orthopaedics, cadaveric dissection allows surgeons to develop critical technical skills, such as using surgical instruments and tissue handling[2]. Another important aspect of cadaver training is to take appropriate protective measures to prevent the spread of infectious diseases[3].

Cadaveric simulation has also been used in orthopaedics for several years, such as virtual reality simulation of fracture treatment incorporating Immersive Virtual Reality (IVR) as a hands-on activity which has become the most developed and validated application[4]. The current model of on-the-job training in hospitals have multiple limitations: time, cost, availability, and access to cases for different patients and fracture types. It is in addition to the discrepancy between patient care, ward duties, and hands-on operative education. Thus, the fact is that the lack of practical training has become a problem and the technical surgical skills of the surgeon directly determine and impact the postoperative outcome and patient safety[5]. Beaven et al.[6] designed an ultra-high-fidelity military cadaveric surgical simulation course to train military medical teams for specific battlefield injuries resulting improvement of medical skills.

A. Background information

Bone fracture simulation in the surgical field has seen advancements, with new testing methods and technologies that allow for more accurate and detailed measurements of bone strength and fracture properties. For instance, the microCT-based finite element analysis[7] combines high-resolution imaging with finite element modelling to accurately predict bones' strength and fracture behaviour. At the same time, the high-speed video camera can capture dynamic loading conditions and nano-indentation, which measures the mechanical properties of bone at the microscale. The animal bone test, such as rodents[8, 9], birds[10], and goats[7] also helps study bone fracture physiology and pathophysiology. However, animal models may not directly reflect human anatomy and physiology. This skill improvement also applies to training using fracture simulation. The story begin with McGinley's [11] in 2003 and later developed by Wegmann et al.[12–16] from the University of Cologne in Germany, who focused on manufacturing pre-fractured specimens to apply in the surgical cadaver training courses to improve the realism of teaching scenarios. Different anatomical parts were researched, including the lower extremities (distal tibia) and upper extremities(distal ulna, radius, and hand). However, several limitations exist, such as accuracy, reproducibility and modularity. The apparatus shown in Figure 1 and Figure 2. fresh-frozen cadaveric upper extremities from individuals were dissected and attached to the device and later fractured by weight impactor. Wegmann et al.[17] reproduced McGinley's test but also induce high-speed video documentation and kinematic analysis. Additional cameras and force sensors were used to record the force data and impact to record impact

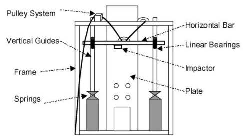

Figure 1: Schematic representation of drop-bench test apparatus from McGinley et al. in 2003[11]

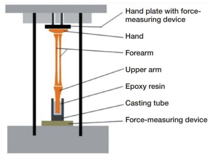

Figure 2: Schematic drawing of the test bench with specimens from Wegmann et al. in 2014[17]

duration. The research group aimed to create kinetic energy of about 210 J. With speed v = 4 m/s and mass m = 21.6 kg, the kinetic energy E can be calculated according to the equation,

$$E = \frac{1}{2}mv^2 \tag{1}$$

Furthermore, damping mechanisms exceeding the damping effects of the specimens themselves were not needed and were not implemented in Harbrecht's research[12, 13].However, the fracture process remained suboptimal. The experimental specimens had different individual characteristics and received diverse impact forces. On the other hand, the joint angles of specimens were inconsistent during the fixation process, which led to different fracture types.

Fractures in the medical field are quite varied and

Figure 3: Fracture simulation in the mechanical setup from Harbrecht 2021[12]

are used to describe a break or crack in a bone based on the location, pattern, and severity of the break, including closed or open fractures, (non-)displaced fractures, partial fractures, complete, avulsion , comminuted, compression, impacted, oblique, spiral, and transverse fractures. The Arbeitsgemeinschaft für Osteosynthesefragen (AO) classification is widely used for classifying fractures[18]. The AO classification system uses a combination of letters and numbers to describe fractures. The first number indicate the anatomic location of the fracture and letter represent the fracture pattern, while the last numbers indicate the degree of displacement[19]. Both 11 out of 12 radius specimen test (92%)[13] and 6 out of 8 tibia fractures (75%)[12] showed that C type fractures were observed for which is complete articular fractures involve the entire joint surface. However, it's important to highlight that discussions with trauma surgeons from the Amsterdam UMC led to the conclusion that C-type fractures, particularly those associated with falls from height, can not represent a natural fracture type.

B. *Problem statement*

The Amsterdam Skill Centre (ASC) represents a cutting-edge simulation training facility dedicated to advancing the pedagogy of Minimally Invasive Surgery (MIS). Its primary objective is to pioneer innovative approaches to surgical education, training, and instruction. At present, ASC is actively engaged in the incorporation and dissemination of progressive methods for surgical learning. ASC currently tends to implement pre-fractured cadaveric specimens in a surgical training course to provide young trauma surgeons with the most realistic surgical experience. However, the fracture apparatus has limitations regarding controlling the type of fracture, consistent and reproducible fractures, and a safe remote-controlled fracture device.

In previous studies[12, 13], it was observed that certain specimens did not fracture during the initial drop-bench test. Instead, multiple impacts, often two or three, were necessary to induce fractures. This necessitated a higher consumption of kinetic energy and resulted in fractures that were less predictable and less stable. On the other hand, the experimental procedures failed to consistently produce identical or desired fracture types. Variations in these fractures were attributed to factors such as the individual specimen's weight, physiological structure, the setup of the experiment, and the axial loading conditions. Furthermore, a significant limitation of the previous testing methodology was the fixation of dissected bones. This approach did not account for the anatomical deformities that specimens might exhibit, which could potentially influence the transmission of axial loads. The experimental apparatus, characterized by an impact stamp mounted on a crossbeam, added an additional mass above the weight of the specimen, thus diminishing the efficient transmission of kinetic energy. Therefore, changes in the device structure and loading method are required to improve fracture efficiency and make the device more controllable and safer.

C. Research objective and questions

This study will give more insights into constructing the fracture device frame and materialization. The main objective can be defined as:

To design a fracture device used for the surgical simulation course of the Amsterdam Skills Centre with a focus on the controllability, modularity, efficiency and safety of inducing natural fractures and to develop and implement the manufacturing of fracture devices.

The main objective can be deconstructed into multiple facets warranting investigation, with corresponding subquestions that can be formulated. The realization of a fracture is contingent upon two primary factors: the impact and material's its brittleness. In order to achieve a fracture simulation that closely mirrors real-world conditions, two crucial elements must be addressed: the fixation of the cadaveric specimen and the control of impact shock applied. The following sub-questions can help build a stable and efficient system:

1. What magnitude of impact energy is required, and what methodologies can be employed to attain it effectively?

2. How can an apparatus be engineered to facilitate the application of predefined torques or forces to the specimen?

3. How to fixate specimen in the device to realize different type fracture?

II. Design Method

A. Delft Design Method

The Delft Design method is a design approach developed at TU Delft. It is a structured and user-centred design method emphasising the importance of understanding the user and their needs throughout the design process[20]. the primary objective is to gain a deep understanding of the problem at hand. It involves defining the design problem and establishing specific requirements, objectives, and constraints. A variety of potential solutions need to be found for the defined problem and multiple design concepts are waiting to be explored. Focusing on shifts to selecting the most promising solution from the conceptual design stage and developing it in greater detail. Creating prototypes and subjecting them to user testing to ensure alignment with user needs. The chosen design concepts are transformed into physical or digital prototypes. These prototypes are rigorously tested and evaluated with users to identify any issues or areas for improvement. After that, refining the design based on feedback and implement the final design solution. The overarching goal of the Delft Design method is to create functional designs that not only fulfill the needs but also align with the desires of the individuals who will use them[20].

B. Design criteria and requirements

Design criteria refer to the set of parameters, standards, and specifications that a design must meet to be successful, which is built based on the customer's needs and requirements as well as technical conditions. The design criteria for this project involve the requirements from the Amsterdam Skill Centre and the design technology in a theoretical framework which mainly involves the following six aspects: **functionality** (the design must perform its intended function reliably and efficiently), **safety** (the design must be safe to use and operate as well as must comply with relevant safety regulations and standards), **durability** (the design must be able to withstand the expected wear and tear associated with its intended use), **cost-effectiveness** (the design must be cost-effective and provide value for money), **ease of use** (the design must be easy to use and require minimal training) and **adaptability** (the design must be adaptable and able to evolve to meet changing needs and requirements)

The project requirements, provided by the Amsterdam Skills Centre and the Surgical

Criteria	Type	Weight
1. The minimum weight of impactor below 25 kg	Functionality	3
2. The maximum impact energy above 200J	Functionality	5
3. Elastic potential energy contributes to impact energy	Functionality	3
4. Minimize energy loss during falling	Functionality	3
5. Ample interior space for specimen	Functionality	4
6. The impact contact surface is changeable	Adaptability	4
7. The impactor weight is changeable	Adaptability	2
8. External protection to prevent bone fragments to fly around	Safety	5
9. The controlled fracture device should be remotely controllable	Safety	5
10. Stable construction structure	Durability	4
11. Training and safety protocol with systematic procedure	Easy of use	2
12. Total cost within 5000 euro	Cost-effectiveness	2

Table I: Design criteria

Criteria	Performance	Score range
1	Above 25 kg; (20, 25] kg; (15, 20] kg; (10, 15] kg ; below 10 kg	1; 2; 3; 4; 5
2	Above 200 J;(150, 200] J; (100, 150] J; (50, 100] J; below 50 J	5; 4; 3; 2; 1
3	(75%, 100%]; (50%, 75%]; (25%, 50%]; [0%, 25%]	4; 3; 2; 1
4	Not only friction loss; high friction loss; low friction loss; no loss	1; 2; 3; 4
5	Example: limbs; torso; intact body	1; 2; 3
6	Changeable; non-changeable	2; 1
7	Changeable; non-changeable	2; 1
8	Translucent; protective; translucent and protective	1; 2; 3
9	Proximal control; remote control	1; 2
10	The multiple of maximum yield strength to stress: 1; 2; 3 and above	1; 2; 3
11	More than 10 steps and 12 hour; within 5 steps and 6 hour;	1; 2
12	[0, 1000); [1000, 2000); [2000, 3000); [3000, 4000); [4000, 5000)€	5; 4; 3; 2; 1

Table II: Performance grading

Department from the Amsterdam UMC. The following table I shows the classified requirement and design criteria. The weight of criteria depends on the importance of the requirement and deisgn construction.

In order to compare the advantages and disadvantages of different concepts more intuitively, the grading based on concept performance in each criterion incorporating with weight can quantify the concepts' feasibility and reliability. The best concept is the one with the highest score by the equation,

$$S = \sum_{n}^{m} P_n * W_n \tag{2}$$

in which S is the total score of the concept, n is the corresponding number of criteria, m is maximum number of criteria, P is the performance score mentioned in table II, W is the criteria weight mentioned in table I. The functionality design criteria is the basis of the system and mainly focus on impactor system, energy, and specimen suitability, including the maximum impact energy, minimum impactor weight, elastic potential energy contribution, energy loss, and available space. Adaptability is about module system design that can improve the versatility of the apparatus, involving changeable impactor weight and impactor. Safety is another important aspect from the user's point of view, the safety distance, impact proof, and remote control are tripe measure to ensure users' and audience ' safety. The fracture device should withstand the expected wear and tear associated with its intended use, the structural stability redundancy ensures the long-term use. For easy of use, a protocol consists of safety instruction and test guide is required to guide beginners. While the budget for the fracture device is 5000 €.

C. Function Tree

A Function Tree is a hierarchical representation of the functions of a system or product. It is a graphical tool used in engineering and design to break down a complex system or product into smaller, more manageable functions. The function tree is typically organized into levels, with the highest level representing the overall system function and each subsequent level representing sub-functions or processes required to achieve the overall function[21]. The project has two main objectives, supported by this visual representation: Fracture execution and Specimen preparation, as shown in Figure 4.

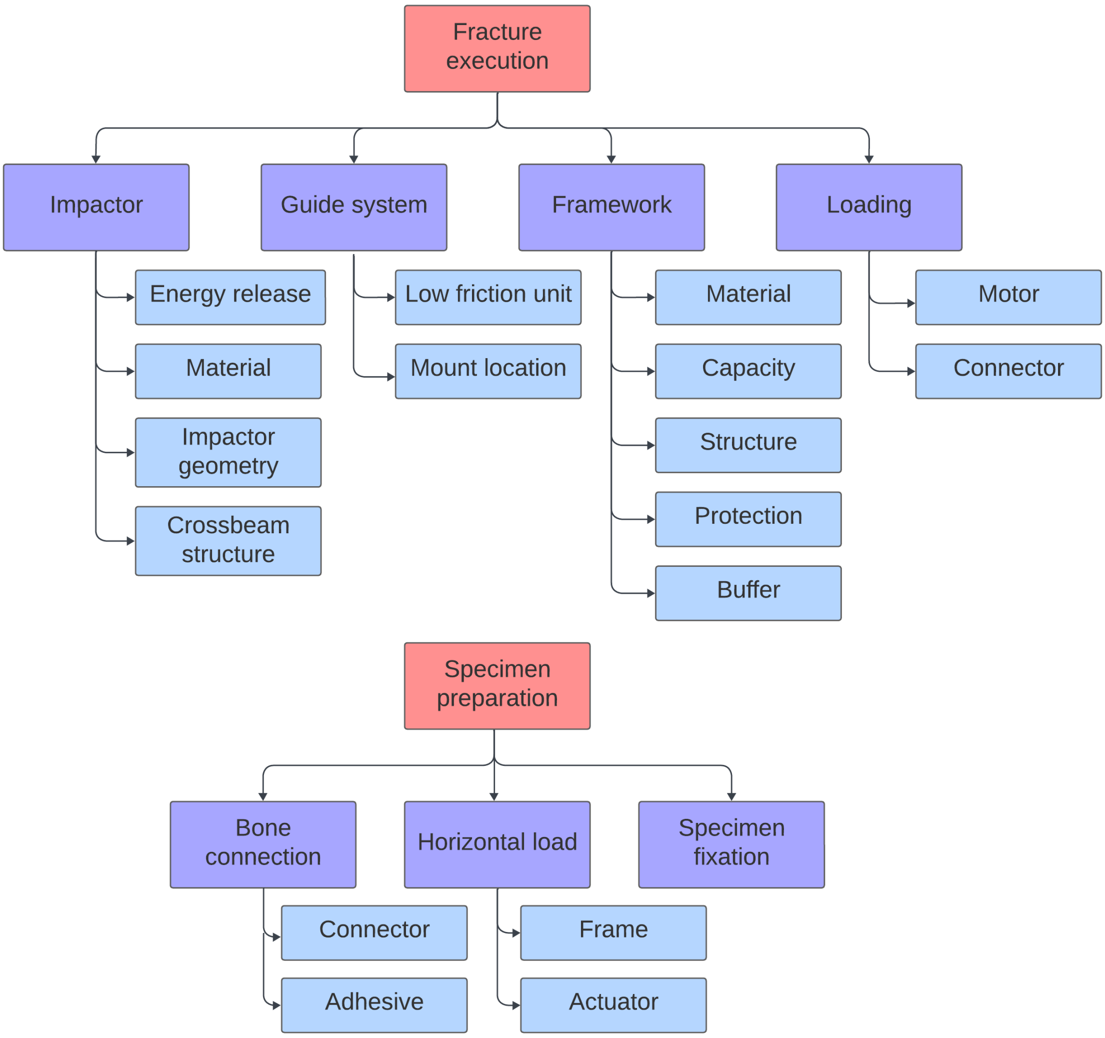

Figure 4: Function tree

1) Fracture execution

The fracture execution function releases stored potential energy and transfers it into impact energy to the specimen, consisting of four sub-functions.

1-1 Impactor This sub-function utilizes kinetic energy to impact the specimen. It has four sub-sub-functions:

- Energy release: This function maximizes the potential energy stored in the system and releases it. The types of potential energy considered in this project include elastic, gravitational, chemical, and electrical potential energy.
- Material: This involves selecting suitable materials for the impactor based on their mechanical and chemical properties, such as weight, corrosion resistance, and yield strength.
- Impactor geometry: The fracturing effect of different impact interfaces is considered when designing the impactor. Therefore, multiple variations of the hammer are listed.
- Crossbeam structure: This refers to the geometry of the drop-weight beam and its connection to the vertical guide.

1-2 Vertical Guide The vertical guide guides the impactor's movement and ensures a frontal collision between the specimen and the impactor. The two critical aspects of building this sub-function are determining the low-friction guides and guide location.

- Low-friction unit: It ensures the smooth movement trajectory of the impactor while minimizing energy loss during the fall.

- Mount location: It influences the fixation method's structure and space.

1-3 Framework This sub-function provides a stable and safe environment for the fracture test. It consists of four components:

- Capacity: It pertain volume of the device that can be suitable for diverse specimens.
- Material: Directly determine the strength of elements and construction stability.
- Structure: It refers to the structure of framework with base and roof.
- Buffer: Can be used for absorbing excess impact.
- Protection and Vision: This refers to the transparent outside cover that prevents bone fragments from posing a hazard in the air.

1-4 Loading: This sub-function provides and increases the potential energy for the weight drop test. It consists of two sub-sub-systems:

- Motor: This refers to the type of power system applied to the system.
- Connector: This introduces the connection method between motor and impactor.

2) Cadaver Fixation and Fracture Type Contribution

Cadaver fixation and fracture type contribution are essential components in this research that involve securing a cadaver specimen and inducing a preloaded force to achieve a specific fracture type, can also be called spceimen preparation. This process involves three critical sub-systems: Bone connection, Cadaver fixation, and Horizontal Load. Moreover, it is vital to consider ethical considerations surrounding using cadavers in research, including obtaining ethical approval and ensuring respectful handling of the cadaver.

2-1 Bone Connection creates a junction between the dissected region of the cadaver and the setup, which consists of two components:

- Connector: A container that connects the fixation mechanism to the dissected bone on the cadaver.
- Adhesive: A sub-sub-system fastens the connection between bone and the Fitting Pot.

2-2 Cadaver Fixation refers to immobilising the entire cadaver while keeping the skin intact.

2-3 Horizontal Load is to introduce additional preload on the cadaver at the beginning of the test and until the weight drop process is implemented. The sub-function contains two components:

- Actuator: The actuator or component that applies force or torque on the cadaver specimen.
- Frame: The region that can be used for actuator mount.

D. Brainstorm and Mind map

This project has integrated both brainstorming and mind mapping techniques. The primary objective of brainstorming is to generate a comprehensive list of ideas, which can subsequently undergo refinement, evaluation, and selection for potential implementation. Conversely, mind mapping involves the creation of a visual diagram to represent these ideas in a structured and interconnected manner.The process of Brainstorming was undertaken collaboratively with the participation of Masie Rahimi and Jaouad Rahouani, yielding a repertoire of conceptualizations. These notions are systematically administered through the employment of a visual mind map, depicted in the accompanying figure 5.

Impactor-Energy release:
The manner in which energy is harnessed and dispensed by a system significantly influences the trajectory of design trends. The concept of Energy release encompasses four distinct categories: Elastic energy, gravitational energy, chemical energy and electrical energy.Elastic potential energy pertains to spring-based systems, encompassing diverse configurations such as spring discs, compression springs, tension springs, and torsion springs. The gravitational potential energy system is exemplified by scenarios involving a weight descent mechanism, wherein an impactor succumbs to gravitational forces and during its descent. Chemical energy is relevant in instances where chemical reactions rapidly transmute into mechanical energy within a concise timeframe. A paradigmatic case in point is the ignition of gunpowder in a bullet, facilitated by a firing pin. The purview of electrical energy spans a broad spectrum of applications, prominently featuring linear actuators and motors as its quintessential manifestations. In the realm of Energesis sub-subsystem design, paramount significance is ascribed to the chief design themes—namely, the maximal energy yield and project budget, both governed by the criteria.Consequently, the application of chemicals and electrical actuators proves less tenable for this system due to the non-reusability of chemicals and the inherent unpredictability associated with energy conversion in chemical

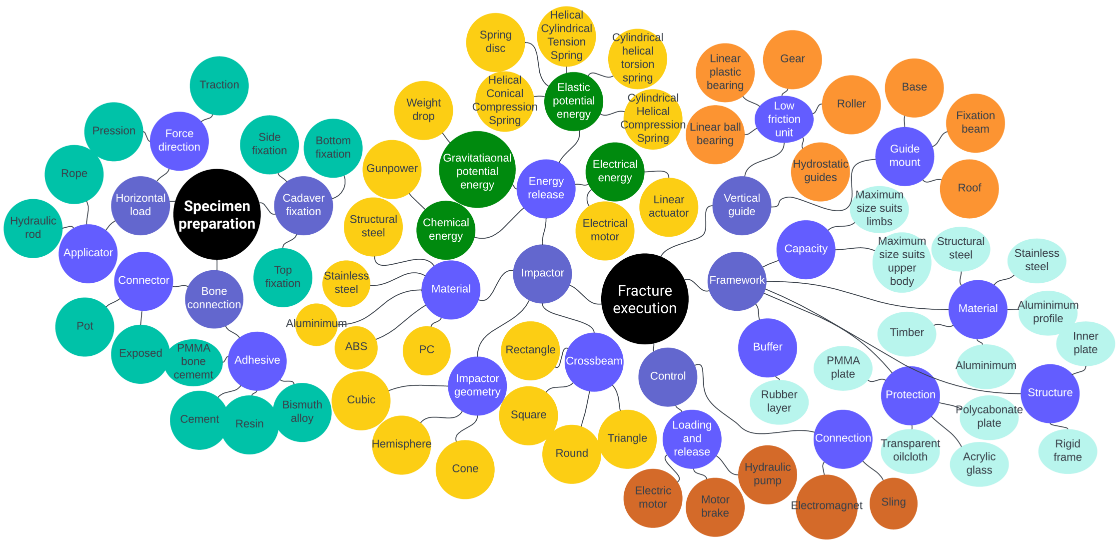

Figure 5: Mind map

processes. Additionally, electrical actuators exhibit an exceedingly low price-to-performance ratio. In contrast, spring-based systems enjoy widespread adoption within industries, affording substantial reservoirs of potential energy albeit necessitating commensurately substantial force inputs. Moreover, the upper threshold of energy attainment through weight drop mechanisms hinges upon the mass and height of the falling object, thus potentially requires larger space.

Impactor-Material:
The mechanical characteristics of the impactor are inherently influenced by its constituent materials. Metals and plastics are frequently employed for this purpose. Notably, stainless steel, structural steel, and aluminum emerge as the predominant choices within the industrial landscape. Stainless steel stands out due to its exceptional resistance to corrosion, while structural steel exhibits a good magnetization effect. Conversely, aluminum is favored for its lightweight nature. On the other hand, ABS, PC, and PVC represent commonly utilized plastic materials with high stiffness, acknowledged for their widespread usage and thin profiles. Nonetheless, it is important to acknowledge that these plastics exhibit a lower stiffness in comparison to steel, thereby leading to more pronounced deformations during impact simulations. Consequently, the utilization of steel and aluminum presents itself as a more robust solution in such scenarios.

Impactor-Head geometry:
The geometry of impact plays a crucial role in influencing not only the transmission of kinetic energy to the specimen but also its deformation, distribution, and extent of damage. These effects are particularly evident when impact loading is introduced. The variables at play revolve around three broad types of contact surfaces: point-plane contact, plane-plane contact, and plane-convex contact. An analogous investigation conducted by Selim Sengel [22] has demonstrated that as the contact surface area increases, there is a subsequent dispersion of force across a wider region of the test sample which means better force and energy delivery.

Impactor-Crossbeam:
The crossbeam is linked to a vertical guide system and add its mass onto the impactor. Therefore, its specific dimensions and proportions will have a direct impact on the overall weight of the impactor. Similarly, the quantity of connectors employed to attach the crossbeam to the vertical guides will play a pivotal role in determining the level of frictional loss experienced.

Framework-Capacity:
As per the discussions held with the Amsterdam Skill Centre's surgical team, it is imperative that the fracture device possesses sufficient internal capacity to accommodate a diverse range of cadaver specimens. This requirement extends beyond merely accommodating limbs such as the

tibia and forearm; it should also be capable of accommodating entire upper body specimens. An insightful study conducted by Anil K Bhat involved the meticulous collection of 13 anthropometric measurements, encompassing the upper limb, grip strength, and three distinct forms of pinch strength, employing a participant pool of 210 volunteers [23]. Notably, the forearm length exhibited considerable variation, spanning from 18.4 cm to 31.3 cm, while the corresponding forearm circumference ranged from 22.5 cm to 34 cm, representing a cylindrical shape. Consequently, the fracture device must possess sufficient dimensions to comfortably accommodate specimens measuring at least 330 mm in length and 11 mm in diameter. Moreover, it's essential to consider the spatial requirements of the other components within the system. Notably, components such as the impactor and the vertical guide system contribute to the overall volume considerations that must be factored into the device's design.

Framework-Material:
The stability of the framework must remain consistent throughout the testing process. Various components will necessitate distinct specifications concerning attributes such as strength, stiffness, weight, dimensions, transportability, and manufacturing conditions. Additionally, cost represents a pivotal consideration; constrained by budgetary limitations, certain designed elements may require streamlining or enhancement. The selection of materials encompasses stainless steel, structural steel, aluminum, and timber. Given its superior durability, metal plate emerges as a more suitable choice than timber for constructing the apparatus.

Framework-Structure:
The structural configuration represents a pivotal factor impacting both the stability of the framework and the efficiency of material utilization. In accordance with the targeted capacity of the equipment, two distinct structural sizes, distinguished by their varying heights, have been tailored. In consideration of the distribution range of force and potential damage, a concept featuring an inner plate has been proposed as a means to curtail metal usage.

Framework-Protection:
The safeguarding shield holds significant importance in ensuring the safety of the spectators. Moreover, it's imperative for the shield to possess transparency, facilitating optimal visibility. Several options are available in this regard, including acrylic glass, plexiglass, transparent oilcloth (PVC), and polycarbonate plates.

Framework-Buffer:
In order to ensure a well-balanced dispersion of force and mitigate the potential impact resulting from erroneous operational procedures, the implementation of a buffering mechanism becomes essential. This is particularly crucial in regions such as beneath the base plate and at the junction where the guide support interfaces with the impactor. Rubber, due to its inherent properties, emerges as a highly effective damping solution suitable for incorporation within the experimental setup.

Vertical guide-Low friction unit:
To minimize energy dissipation due to friction during descent, the implementation of low-friction mechanisms becomes imperative. Several options exist, including linear plastic bearings, linear ball bearings, gears, rollers, and hydrostatic guides. Among these choices, linear bearings are frequently preferred. However, it's worth noting that gear systems demand substantial lubrication, hydrostatic guides necessitate the incorporation of an air pump and additional power, and rollers exhibit inferior performance compared to bearings.

Vertical guide-Guide mount:
The stability of guides determines a consistent trajectory of the impactor during its descent. Moreover, the positioning of these guides significantly impacts the methodology employed for specimen fixation as well as its applicability across various specimen types. The selection of guide mounting points encompasses three potential options: the base, roof, and fixation beam. The base mount option stands out for its simplicity and inherent stability, while the utilization of the beam mount necessitates a robust and steadfast architectural configuration.

Loading-motor:
The Power source depends on the energy release system.Hence, we are considering the utilization of an electric motor with a braking system, as well as a hydraulic press. Unlike a motor on its own, which cannot come to a halt or be immobilized at a specific position when subjected to external forces,

the incorporation of a motor brake enables such functionality. Meanwhile, a hydraulic press offers the capability of delivering substantial force output.

Loading-Connector:
The connection mechanism is engineered to establish a linkage between the impactor and the loading and release system. The impactor has the capability to be seamlessly affixed to the motor traction wire through employment of a sling, hook, or an alternative tangible fastening mechanism. The hydraulic press is interlinked with a spring system, whereby the inherent potential energy of the springs can be transmitted to the impactor. Leveraging the electromagnetic principle, electromagnets exploit the inherent magnetizability of iron, with the caveat that this phenomenon gradually attenuates upon power cessation . This property ensures that the impactor can descend without reliance on a direct physical linkage, thereby mitigating energy dissipation.

Cadaver fixation:
The cadaver fixation method restricts the specimen's movement during testing to just one or two degrees of freedom. Specifically, these movements involve linear motion along the vertical (z) axis and combined linear and rotational motion along the z-axis. Implementing such movements within the cadaver fixation necessitates supplementary mechanisms, such as additional crossbeams, plates, or ropes. The cadaver fixation approach encompasses three distinct methods: top fixation, bottom fixation, and side fixation. The top fixation method is based on prior research[12], involving vertical fixation of the cadaver's upper segment. In contrast, we have opted for a novel approach that reverses the fixation point, referred to as bottom fixation. Meanwhile, side fixation serves to curtail specimen rotation while introducing a predetermined torque to the cadaver. Our aim in employing side fixation is to assess its potential in inducing fractures at specific desired locations.

Bone connection-Connector:
To implement the top and bottom fixation methodology, it may be necessary to introduce supplementary connecting components to the specimen. We contemplate two approaches: firstly, the impactor could interface directly with the uncovered dissected bone; alternatively, the bone could be affixed to a suitable container which is subsequently inserted into a sliding bearing system which allows moving up and down.

Bone connection-Adhesive:
The adhesive substance are used to connect bone with connector. This notion has been explored in prior studies through various approaches such as bone cement [9, 12], resin[8, 17], and bismuth alloy[7]. As discuss with surgery department from Amsterdam Skill Centre, we also take cement in to consideration due to its cost-effectiveness.

Horizontal load:
The force applicator possesses the capability to exert either traction or compressive force upon a cadaveric specimen, thereby achieving a predetermined torque. Our contemplation extends to the utilization of a hydraulic rod for applying compressive force or a rope for inducing traction.

E. Conceptual Design

The initial phase of concept design involves merging ideas enumerated in brainstorming sessions to forge two feasible conceptsm, as shown in Figure6 . These concepts diverge significantly in their inspiration and intent. The first concept revolves around enhancing device compatibility. This required ensuring that the equipment could seamlessly accommodate various region of cadaver specimen, enabling the simulation of various fracture effects. Additionally, the design incorporates modular components, allowing for a higher degree of flexibility and adaptability. This modular approach allows for rapid customization and adjustment to meet the changing requirements of the simulation process. The second concept, on the other hand, took a different trajectory, focusing on component compression to make the apparatus small and mobile. This design improves ease of transportation and maneuverability by reducing the overall size and weight of the assembly. This design route prioritizes compactness and portability, making it a practical choice for scenarios where mobility and space efficiency are paramount. These two distinct conceptual routes represent thoughtful considerations that address varied aspects of equipment functionality and practicality. Each approach offers unique advantages and their own route shown in Table III.

The differentiating factor between the two conceptual designs primarily pertains to the energy collection method employed by the impactor mechanism. In the first concept, energy collection

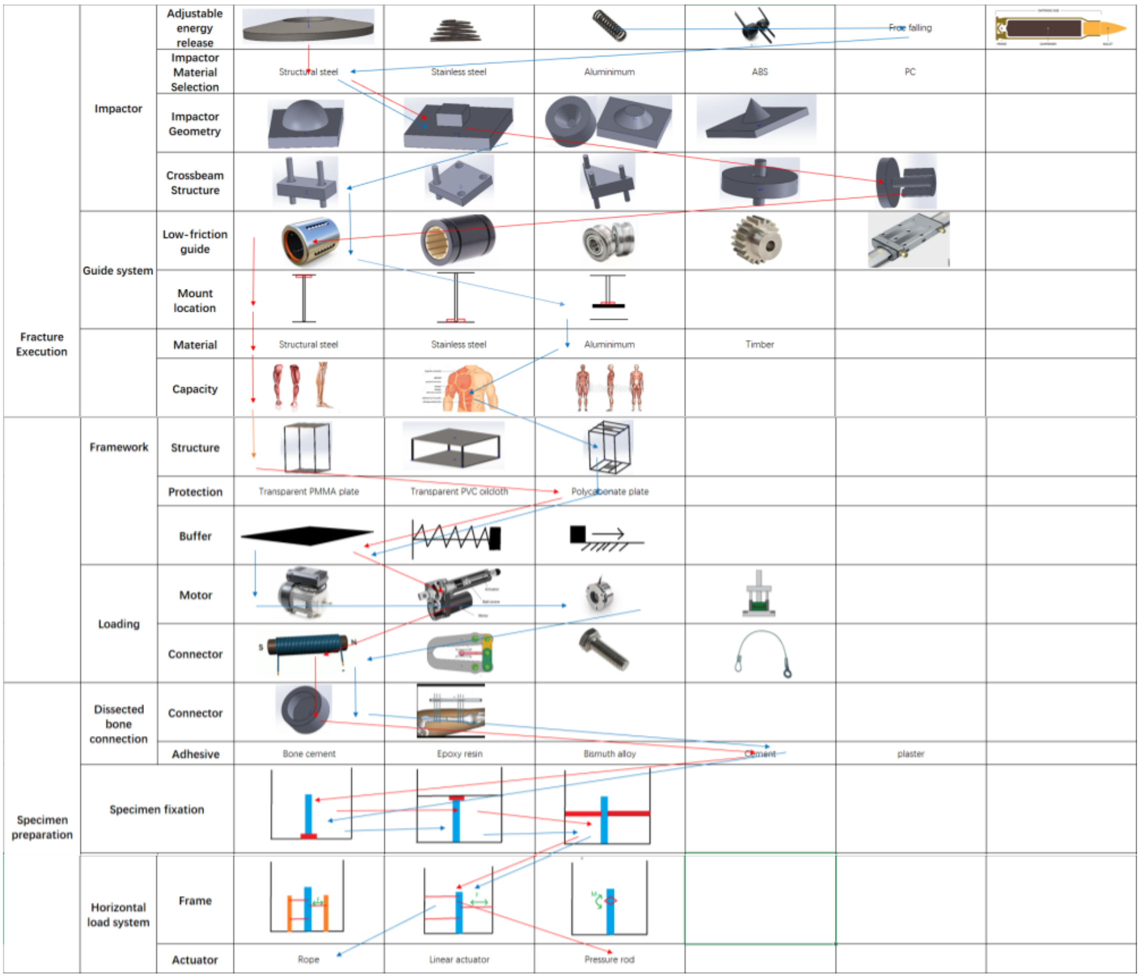

Figure 6: Morphological chart

Function	Concept 1	Concept 2
Energy release	Weight drop & Helical compression spring	Spring disc
Impactor material	Structural steel	Structural steel
Impactor geometry	Modular (Cubic as usual)	Modular (Cubic as usual)
Crossbeam	Rectangle with two guide hole	Round
Low friction unit	Linear ball bearing	Linear ball bearing
Guide mount	Fixation beam & roof	Roof
Capacity	Maximum size suits upper body	Maximum size suit limbs
Structure	Rigid frame with inner plate	Rigid frame
Frame material	Aluminium profile, Aluminium	Stainless steel
Protection	Polycarbonate plate	Polycarbonate plate
Buffer	Rubber plate	Rubber plate
Loading & release	Electrical motor with brake	Electrical motor
Connection	Electromagnet	Electromagnet
Cadaver fixation	Top, bottom, and side fixation	Top, bottom, and side fixation
Adhesive	Cement	Cement
Bone Connector	Pot	Pot
Applicator	Rope	Hydraulic rod

Table III: Conceptual design

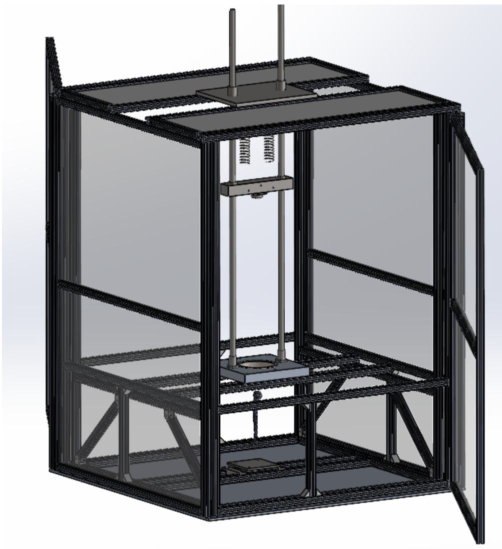

Figure 7: Schematic drawing of Concept 1

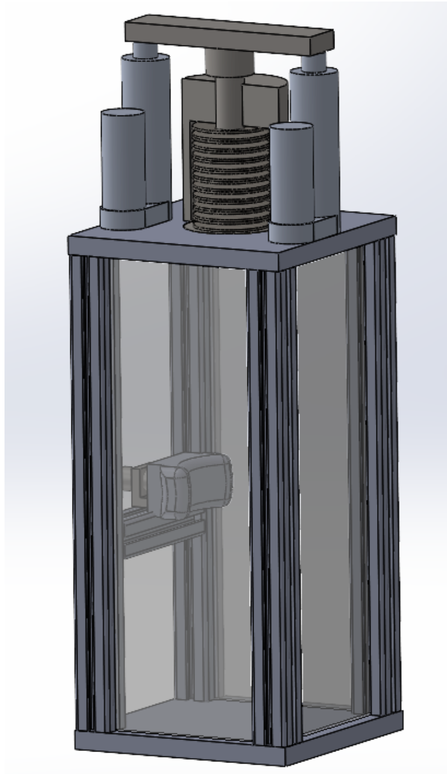

Figure 8: Schematic drawing of Concept 2

hinges on the elastic potential energy stored in a compression spring as well as gravitational potential energy of the impactor itself. This dual-source energy conversion approach is engineered to increase maximum potential energy that can be transformed into kinetic energy needed for the impact. This method offers a more robust and adaptable energy supply for the impactor. In stark contrast, the second concept adopts a more streamlined approach to store energy. It relies mainly on the elastic potential energy stored in a spring disc. This design choice significantly minimizes the external space requirements of the device, making it more compact and spatially efficient. However, it does come with certain trade-offs, as it may be somewhat limited in material frame construction strength and availability on specimens compared to the first concept. Essentially, while both concepts aim to achieve the same goal, their energy loading strategies differ. The first concept prioritizes versatility and power, harnessing multiple energy sources, while the second opts for a more space-efficient design, despite potential limitations in impact capability. The concepts are visualized in Solidworks. As shown in Figure 7 and Figure 8.

1) Concept grading and visualization

The grading of concepts is determined by their anticipated performance relative to each design criterion, and the overall grade can be computed using the equation 2 presented in Table IV. It is noteworthy that the cumulative grade for Concept 1 surpasses that of Concept 2, with the most significant disparities in performance grades observed for Criteria 5 and 10. This discrepancy is attributed to the Amsterdam Skill Centre's stringent requirement for ample interior space, which is especially critical. Additionally, Spring disc, designed for Concept 2, necessitates a minimum force of 4000 N and a contact stress of 1000 MPa, both of which surpass the yield strength threshold of structural steel, stainless steel and aluminum which are commonly used.

Concept 1 was rendered using Solidworks software. The experimental setup primarily comprised aluminum profiles and was situated atop a 6 mm thick black rubber polyethylene foam sheet designed to absorb impact forces effectively. To ensure optimal force distribution, an 400mm X 400 mm aluminum base plate was securely affixed between two profiles at the center bottom of the apparatus. The height-adjustment mechanism featured four 1360mm-long profiles and four 400mm-long profiles, enabling height adjustments by altering the angle between the support profile and the ground. A fixation crossbeam was positioned at the midpoint of this height-adjustable mechanism. This crossbeam facilitated the vertical guides, offering versatility for accommodating various cadaveric specimens, diverse fixation methods, and multi-axial pre-loading. Constructed from aluminum, the fixation crossbeam featured a central aperture measuring 185mm in diameter, and it was fitted with a Teclite bearing secured within a cement pot. Two vertical stainless steel guides, each measuring 1900 mm in length and 30 mm in diameter, were affixed to the fixation crossbeam. These guides determined the trajectory of the impactor's descent, ensuring a frontal collision between the fitting pot and the impactor for efficient force transmission to the specimen. The impactor itself consists of a steel crossbeam and a modular steel hammer. Its minimum weight was set at 15 kg, with the option to adjust this weight by adding supplementary weight plates. Four linear ball bearings were integrated into both the impactor and the roof plate, allowing for spring compression and impactor drop, facilitated by the two stainless steel guides and two aluminum guides. Additionally, the spring system was introduced to enhance the maximum impact energy output, capable of generating a maximum of 50 joules of energy under full compression.

Criteria	C1	C2	Weight	G1	G2
1	4	5	3	12	15
2	5	5	5	25	25
3	3	4	3	9	12
4	3	3	3	9	9
5	3	1	4	12	4
6	2	1	4	8	4
7	2	1	2	4	2
8	3	3	5	15	15
9	2	2	5	10	10
10	3	1	4	12	4
11	2	2	2	4	4
12	1	3	2	2	6
Total				122	110

Table IV: Concept grading

III. Designing details and analysis

A. Analysis: Elastic energy estimation and spring system

1) Spring Design and potential energy storage

A spring system is a physical system consisting of one or more springs connected. Springs are mechanical devices that are designed to store and release energy by deforming under the application of an external force. The spring design phase involves selecting the spring type and considering the corresponding force, size and maximum stored energy which influence the performance of the fracture device. In this study, cylindrical helical compression springs and spring discs are investigated and discussed for their possible application in the energy release system. Amatec and Belleville Springs offer the spring parameter and data for this study.

Cylindrical helical springs: Cylindrical helical springs are the most widely used and can be divided into helical compression springs, helical extension springs, and helical torsion springs according to load. Springs with cylindrical shapes are typically made by helically coiling wire with a constant clearance between the active coils. These types of springs are effective at absorbing external counter-acting forces that are applied against each other in their axis. In this study, we use helical compression springs, which is typically axial load linear spring. The spring is endowed with internal stress, which is the state under the minimum load. According to the function of the spring, there are four basic spring states:

The elastic potential energy of one single cylindrical helical compression spring at maximum operational loading can be calculated based on the equation:

$$P = \frac{1}{2}k(L_0 - L_8)^2 \tag{3}$$

P is the maximum working potential energy, k is the stiffness constant of the spring, L_0 spring length at free state, and L_8 is the spring length at fully load state. The parameters are shown in figure 9.

Spring Discs: Spring discs, also called Belleville washers, are mechanical components used in various applications to provide high load-bearing capacity in a compact space. These washers are made from thin, conical-shaped metal discs with a slightly curved profile, and they can be stacked together in series or parallel to form a spring pack. The desired level of spring force can be achieved by compressing or expanding the pack. Spring discs offer versatility in operating parameters, as the size and stacking arrangements can be varied to achieve a range of spring forces.

Spring State	Description	index
Free	the spring is not loaded	0
Preload	the spring is exposed to minimum operational loading	1
Fully load	the spring is exposed to maximum operational loading	8
Limiting	the spring is exposed to the limit load – given by design limitations (eg,compression of the coil spring to bring all coils into contact)	9

Table V: individual parameter index[24]

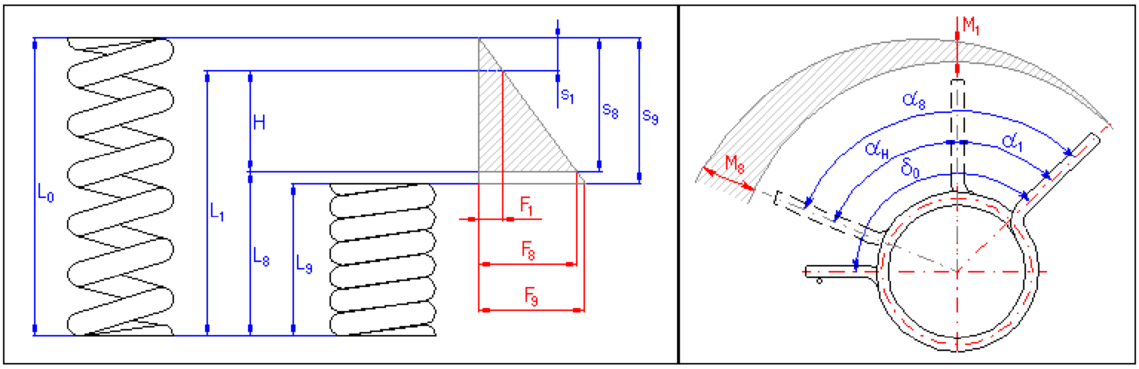

Figure 9: Index and state force (Left: helical compression spring; Right: helical torsion spring)[24]

They are commonly used in valves, clutches, and shock absorbers applications. The spring disc has three arrangement methods: parallel, series, and combined[24, 25], shown in Figure 10. In a parallel arrangement, the washers are stacked parallel, resulting in a higher spring constant and even stress distribution across each washer. In a series arrangement, the washers are arranged against each other, resulting in a lower spring constant, but each washer experiences the same stress as a single washer. A combined arrangement uses both series and parallel arrangements to achieve a desired level of stiffness.

The axial force and four edge stresses relation are as follows:

$$Force\ F = \frac{4Et^3s[(\frac{h}{t}-\frac{s}{t})(\frac{h}{t}-\frac{s}{2t})+1]}{(1-\mu^2)K_1D^2} \tag{4}$$

$$\sigma_I = \frac{4Ets[K_2(\frac{h}{t}-\frac{s}{2t})+K_3]}{(1-\mu^2)K_1D^2} \tag{5}$$

$$\sigma_{II} = \frac{4Ets[K_2(\frac{h}{t}-\frac{s}{2t})-K_3]}{(1-\mu^2)K_1D^2} \tag{6}$$

$$\sigma_{III} = \frac{4Ets[(K_2-2K_3)(\frac{h}{t}-\frac{s}{2t})-K_3]}{(1-\mu^2)K_1D^2\delta} \tag{7}$$

$$\sigma_{IV} = \frac{4Ets[(K_2-2K_3)(\frac{h}{t}-\frac{s}{2t})+K_3]}{(1-\mu^2)K_1D^2\delta} \tag{8}$$

$$Diameter\ ratio\ \delta = \frac{D}{d} \tag{9}$$

$$K_1 = \frac{(\frac{\delta-1}{\delta})^2}{\pi(\frac{\delta+1}{\delta-1}-\frac{2}{\ln\delta})} \tag{10}$$

$$K_2 = \frac{6(\frac{\delta-1}{\ln\delta}-1)}{\pi\ln\delta} \tag{11}$$

$$K_3 = \frac{3(\delta-1)}{\pi\ln\delta} \tag{12}$$

D is outside diameter, d is inside diameter, E is the modulus of elasticity in tension, H is disc height, h is unloaded cone height (h = H - t), t is the disc thickness, μ is Poisson's ratio, s is spring deflection, shown in Figure 11.

In contrast to helical springs, the majority of spring discs exhibit nonlinear (degressive) working characteristics. The load-deflection curve of a single spring is not linear. Its shape depends on the ratio of the cone height. As the deflection increases, the force moment arm shortens and force required increase sharply when deflection exceeds 75%, the deviation from the theoretical increases sharply. Therefore, the force-deflection predictability is limited to 75% of total deflection.[26] Consequently, it is not possible to compute potential energy using the conventional linear equation as outlined in Equation 3. Instead, the estimation of the working elastic potential energy P can be formulated as follows:

$$P = \int Fs \tag{13}$$

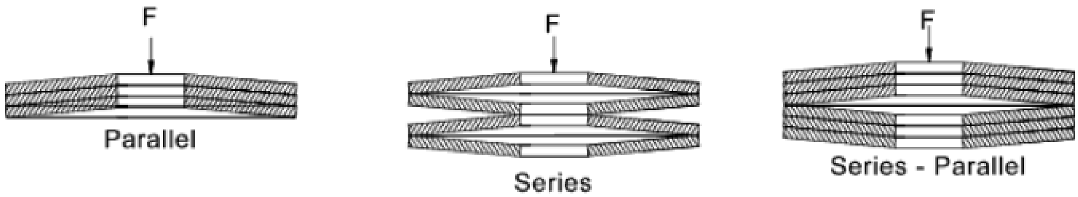

Figure 10: Spring disc arrangement[25]

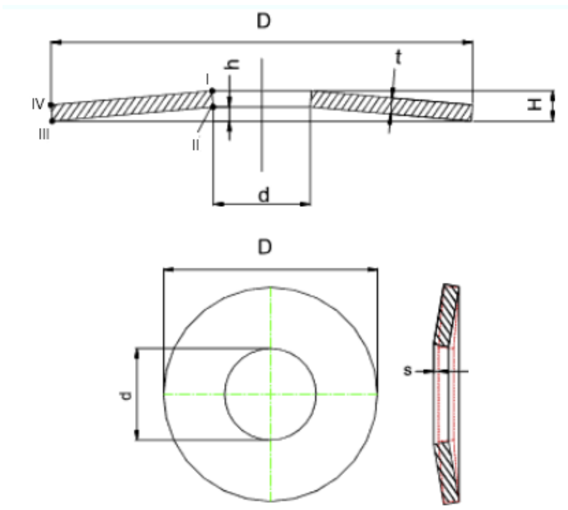

Figure 11: Spring disc[25]

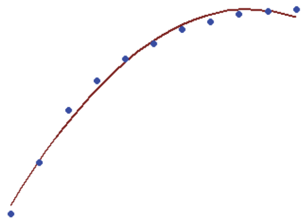

Figure 12: Curve fitting

Creating a load-deflection data sheet involves the acquisition of axial force data for spring discs, which is then measured or provided at various deflection levels, typically at 15%, 30%, 45%, 60%, 75%, and 90% of the maximum deflection. The process of curve fitting is employed to identify a mathematical function, usually in an analytical form, that best aligns with this dataset, as depicted in Figure 14. This curve fitting procedure serves the purpose of estimating a polynomial function that can be subsequently utilized in the integration process outlined in Equation 13. Specifically, when we refer to polynomial regression, we are addressing the scenario where we aim to fit a polynomial of a particular order denoted as d to our dataset as:

$$\begin{gathered} y = ax + b, d = 1 \\ y = ax^2 + bx + c, d = 2 \\ y = ax^3 + bx^2 + cx + d, d = 3 \\ \dots\dots \end{gathered} \tag{14}$$

2) Material elasticity and plasticity

Material elasticity refers to the ability of a material to deform reversibly when subjected to an external force and then return to its original shape and size when the force is removed. There are linear elasticity, typically for metal, and nonlinear elasticity, typically for rubber polymers. Base on current design background of fracture apparatus material that only metals are involved. We only discuss linear elasticity. The characteristics of linear elasticity are reversible, instantaneous, and no dissipation.

$$\theta = E\epsilon \tag{15}$$

in which θ represents stress, E represents Young's modulus, and ϵ represents strain, it is important to note that the Young's modulus (E) remains constant. Consequently, the relationship between strain and stress is consistently proportional, as depicted in Figure 13. Conversely, plasticity refers to a material's capacity to undergo enduring deformation when exposed to an external force surpassing its elastic limit. This behavior is illustrated in Figure 13, where unloading results in an external strain denoted as ϵ^e. It is imperative to avoid such unloading scenarios in system design. The concept of yield strength, denoted as θ_y, carries significant mechanical significance, particularly in the realm of metals and alloys. This parameter signifies the maximum stress level that a material can endure without incurring permanent deformation. Therefore, the maximum stress appear in the component should not exceed its yield strength during static and dynamic analysis.

No.	75% Deflection displacement	Force	Stress III	Estimated energy
D803125	2.1 mm	7239 N	1081 N/mm^2	9.47 J
D71362	1.9 mm	5144 N	1342 N/mm^2	6.59 J
D633118	1.76 mm	4238 N	1351 N/mm^2	6.45 J
D602042	1.58 mm	4727 N	1044 N/mm^2	4.55 J

Table VI: Spring disc at 75% deflection

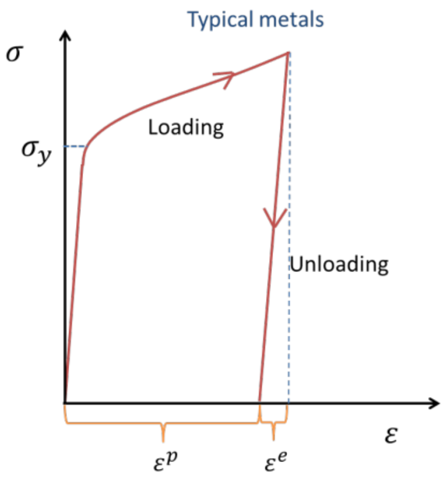

Figure 13: Metal elasticity and plasticity

3) Analysis

In accordance with data gleaned from prior research efforts, it has been established that the highest achievable impact energy stands at an impressive 210J. These findings, as corroborated by studies such as those conducted by Ott et al.[12], Wegmann et al.[13] in their pioneering work on inducing impact energies, and further simulations[14], and crack propagation [16], collectively underscore the upper limit of impact energy attainment. The prevailing evidence strongly suggests that even the observed kinetic energy of 184 joules may be excessive when it comes to generating realistic fractures in human cadaver specimens. Given these compelling findings, there emerges a reason for constraining the maximum impact energy output to a more conservative 200 joules. To attain the desired upper limit of 200J for impact energy output, it is imperative to meticulously calculate and design the output systems for both conceptual approaches. The calculation of impact kinetic energy for these two systems can be effectively based on the following fundamental formula:

$$\begin{gathered} I_1 = M_1 g h, \ (h \leq h_0 - t) \\ I_1 = M_1 g h + \tfrac{1}{2} k (h - h_0 + t)^2 \\ I_2 = M_2 g s + \int_0^s F x dx \end{gathered} \tag{16}$$

in which subscript 1 and 2 refers to the first and second concepts, I is the transformed impact energy, M is the mass of the impactor, g is gravitational acceleration, h is the vertical distance between impactor and specimen, h_0 is the vertical distance between compression spring and specimen, s is the deformation of the spring disc,t is the total thickness of the impactor, F is the force function, which is estimated using a third-order cubic polynomial regression.

To identify the most suitable spring disc and compression spring, we conducted a simple market search. In the context of the spring system, it is essential to consider that a higher stiffness results in shorter and smaller springs but necessitates a greater compression force. This trade-off implies a more efficient and powerful loading unit, albeit at a higher cost. Moreover, the arrangement of springs, whether linearly stacked or in parallel stacks, can enhance the upper limit of the system's elastic energy. This allows for the utilization of smaller springs to achieve the effect of larger single one. We focused our attention on Disc Springs conforming to DIN 2093, which exhibit consistent parameters in the market. Among these, we identified typical four specific spring disc types with the minimum force at 75% deflection within their respective series: D803125, D71362, D602042, and D633118, in which data offered by Belleville[27]. Subsequently, we employed the "fit" function in Matlab to estimate the corresponding force functions, as illustrated in Figure 14. This analysis was followed by the utilization of mathematical integration techniques to compute the elastic potential energy within each individual spring disc by equation 13 and stress III by equation 7.

The computed energy and stress values for individual spring discs at 75% deflection are tabulated in Table VI. It is noteworthy that the stress levels calculated for each spring disc at this deflection threshold exceed the threshold of 1000 MPa. However, it is essential to contextualize these findings within the framework of material

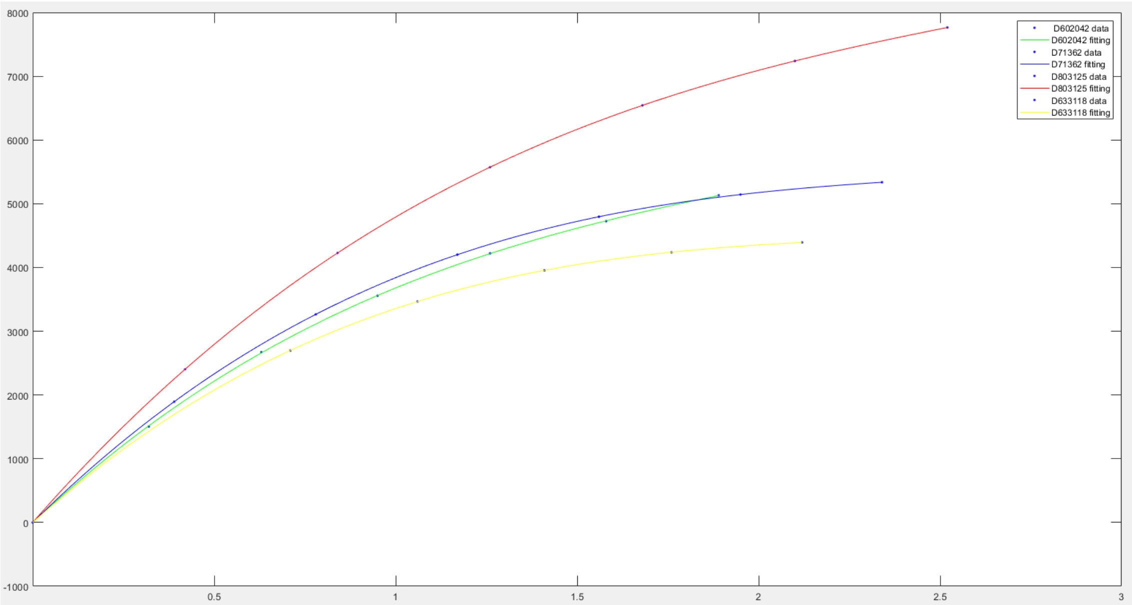

Figure 14: Spring disc data curve fitting

properties. Steel, as a common material for spring components, exhibits a yield strength range of approximately 200 to 700 MPa. For example, stainless steel 304L has a yield strength of 205MPa at a temperature of 20°C, structural steel S235 boasts a yield strength of 235 MPa, while high-strength steel A514 demonstrates a remarkable yield strength of 700 MPa. In light of this, it is evident that employing spring discs in a spring system tasked with sustaining high forces will likely result in steel plastic deformation.

B. Analysis: Finite Element Analysis of impact simulation

1) Impact test

Impact testing serves the purpose of assessing the energy absorbed or the energy necessary to cause a unit under test (UUT) to fracture. Consider, for instance, a scenario involving a head-on collision between two objects, similar to a car crash. By applying the work-energy principle, which states that the average impact force multiplied by the distance traveled is equal to the change in kinetic energy, design engineers have the capability to mitigate the impact force experienced during a car collision. They achieve this by increasing the stopping distance, typically through the incorporation of specialized 'crumple zones' designed to absorb and dissipate kinetic energy.

A straightforward experimental procedure for quantifying the impact force concerning displacement involves integrating the force-displacement curve to obtain an energy-based measurement[28]. This method relies on the fundamental principle of work-energy, where the potential energy (P) prior to an event is equated to the kinetic energy (K) following the event.

$$P = K \tag{17}$$

And for weight drop test, the relationship between drop mass m, falling height h, acceleration of gravity g, and velocity v is

$$\begin{aligned} mgh &= \tfrac{1}{2}mv^2 \\ v &= \sqrt{2gh} \end{aligned} \tag{18}$$

Force-distance To determine the expected force during an impact, we can rely on the concept that the net work done during the impact is equivalent to the product of the average force of impact and the distance traveled during the impact. In the context of a drop test, where the initial velocity of the impactor is zero, the transferred energy is equal to the initial potential energy. Assuming that it is feasible to measure the vibration resulting from the impact, denoted as "d," we can calculate the force as follows:

$$F = \frac{mgh}{d} \tag{19}$$

It is essential to note that this principle assumes that the impactor is completely rigid and remains in continuous contact with the specimen throughout the entire process[28]. Any energy losses due to factors such as friction, heat, noise, and deformation are disregarded in this calculation.

Force-time By employing the final velocity derived from the conservation of energy Equation18 and the speed reduce to zero after collision, we can proceed to determine the resulting average impact acceleration. This acceleration parameter is contingent upon the pulse width of the force-time curve and necessitates an estimated value derived from diverse material types, analogous to the approach used for estimating impact distance. The calculation for impact acceleration (a) is performed by considering the change in velocity over the duration of the pulse width.

$$a = \frac{dv}{dt} = \frac{dv}{t_{pulse}} = \frac{\sqrt{2gh}}{t_pulse} \tag{20}$$

and force-acceleration relationship is,

$$F = ma \tag{21}$$

2) FE Analysis

Finite element analysis (FEA) stands as a pivotal computational technique employed extensively within the fields of engineering and physics. It serves the critical purpose of scrutinizing and emulating the intricate responses exhibited by complex structures and systems. In this context, a fracture device designed to disperse 200 joules of impact energy necessitates a robust and resilient construction, which fundamentally underpins the safety of its users. The paramount consideration here revolves around the device's ability to withstand not only its own weight but also the forceful energy release during impact events. The dynamic analysis steps in to scrutinize the transient responses that transpire during impact test. It is specifically tailored to evaluate the device's performance under rapidly changing conditions, such as those experienced during energy release. Dynamic analysis allows for the prediction of stress, strain, and deformation patterns as the device absorbs and dissipates the impact energy. FEA consists of three main phase: preparation, construction, and analysis, as shown in Figure 15.

Preparation phase: The fracture device has been sketched using Solidworks, a computer-aided design (CAD) software, as depicted in Figure 27. This software enables the creation of three-dimensional (3D) models by amalgamating individual components or parts into an assembly.

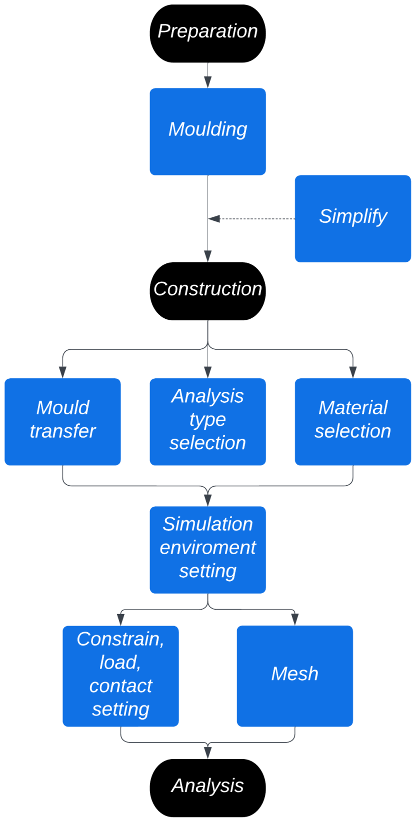

Figure 15: Finite element analysis flowchart

Nevertheless, owing to the intricate characteristic of the fracture device's structure, analyzing the entire assembly can be a time-intensive and messy process for the computer. Thus, in order to expedite the simulation and improve the accuracy, it becomes imperative to employ simplification of 3D model, as shown in Figure 36 in appendix.

Construction: The CAD model is going be transferred into the internal model of Ansys. In the case of the impactor, the Explicit Dynamic test incorporates the time-dependent characteristics of applied loads and boundary conditions, as illustrated in Figure 16 and Figure 17. This test furnishes valuable insights into how the system's parameters evolve over time, encompassing aspects such as displacements, velocities, accelerations, and stresses. Regarding the primary frame and support system, which includes the base support and fixation crossbeam, static simulations enable us to ascertain stress distribution, strain patterns, displacements, and other pertinent parameters within the structure when it is in a state of static equilibrium. Our focus revolves around investigating the mechanical properties of available materials, namely stainless steel AISI 304 L, structural steel variants S235 and S355, and aluminum 6082-T6. During the simulation process, it is imperative to define stress and constraint conditions for each component based on real-world considerations, as well as contact between different structural elements. The impactor and hammer were initially imparted with a specific initial velocity, and the velocity experienced variations across different tests due to fluctuations in the weight of the impactor, indicated in table VII. However, it's noteworthy that the ultimate kinetic energy of the impactor consistently remained at 200 Joules. As for mesh sizing, we employ an automatic sizing approach tailored to the complexity of the assembly. This approach allows for the application of distinct mesh sizes and shapes to various components based on their geometry and volume in one simulation.

Analysis: This phase aims to assess the stress levels, displacements, and overall deformation experienced by the components. Additionally, during the analysis, it involves verifying whether the designed parts exceed yield strength criteria and permissible tolerances. The maximum von-Mises stress was recorded in the table VII and details in appendix section A.

Figure 16: Ansys workflow chart

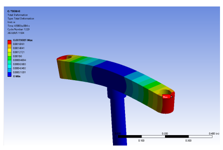

Figure 17: Ansys Explicit Dynamic analysis

length	width	thickness	Velocity	Stress
680 mm	80 mm	60 mm	4 m/s	277.9 MPa
680 mm	80 mm	70 mm	3.723m/s	264.4 MPa
680 mm	80 mm	80 mm	3.498 m/s	177.7 MPa
680 mm	80 mm	100 mm	3.147m/s	93.1 MPa
680 mm	100 mm	80 mm	3.095m/s	165 MPa
680 mm	120 mm	80 mm	2.79m/s	147.7 MPa
680 mm	160 mm	80 mm	2.359m/s	118.3 MPa
580 mm	80 mm	80 mm	3.814 m/s	127.4 MPa
480 mm	80 mm	80 mm	4.216 m/s	103.9 MPa

Table VII: Explicit dynamic finite element analysis of simplified impact test model

As mentioned in previous analysis, the yield stress for structural steel S235 is 235 MPa and stainless steel 304L IS 205 MPa. The impactor could be regarded as a cuboid. The increase of width and thickness lead to the decrease of velocity and increase in inertia, and the stress become smaller. The increase of length lead to the increase in velocity and decrease of force moment, and the stress become smaller. The minimum value is from 480-80-80 which is 103.9 MPa. A further test of the improved model, in which a stainless steel pot between impactor and specimen was introduced and tested. The impact speed is set to 5.3m/s The Maximum stress in impactor is 386 MPa and in pot is 246 MPa as shown in appendix Figure 55.

C. *Research on bone characteristics and conjecture about introducing preload force*

Bone is a type of connective tissue that makes up the skeleton of vertebrates, including humans. It is a complex and dynamic living tissue that provides structural support, protects vital organs, and serves as a reservoir for minerals such as calcium and phosphate. Bone tissue is composed of a mineralized extracellular matrix primarily made up of collagen fibres and hydroxyapatite crystals[29]. The matrix gives bone strength and rigidity, while the collagen provides flexibility and resilience. As shown in Figure 18, bone also contains various types of cells, including osteoblasts, osteocytes, and osteoclasts, which are responsible for forming, maintaining, and remodelling bone tissue. There are two main types of bone tissue: compact bone, also called cortical bone, and spongy bone[30]. Compact bone is dense and forms the outer layer of bones, while the spongy bone is less dense and makes up the inner layer of bones. Bones are also classified based on their shape, with long bones such as the femur and humerus, flat bones such as the skull and scapula, and irregular bones such as the vertebrae and pelvis.

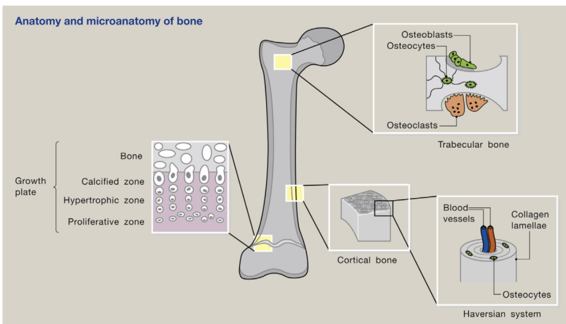

Figure 18: Bone structure and metabolism[30]

Fracture mechanics constitutes the scientific exploration of the behavior exhibited by cracks and other structural flaws within materials, coupled with an analysis of their ramifications on the structural integrity and longevity of constructions. Diverging from material yield, the occurrence of fracture arises at points where stress becomes concentrated or emerges in proximity to pre-existing cracks[31]. The domain of fracture mechanics has sought to delineate the resistance of bone to fracture by quantifying critical parameters, primarily the stress intensity factor and the strain energy release rate, which are measured at the instigation of a fracture crack[32]. Within the context of cortical bone, a composite material, the accrual of microcracks, 30–100 micrometer, emerges as a consequence of extended periods of mechanical loading, thereby contributing to bone fatigue and stiffness and strength have been shown to decrease as the number of microdamages in bone increases[33]. A pivotal facet underpinning the robustness and tenacity of bone lies in its remarkable capacity for undergoing substantial inelastic deformation. The occurrence of microcracking constitutes a critical phenomenon that accompanies the inelastic deformation of both bone and nacre[34]. Research conducted by Peter Zioupos[35] has demonstrated that bone subjected to high strain rates displays brittle behavior, while specimens subjected to lower strain rates exhibit enhanced toughness, with the occurrence of microcracking exhibiting an inverse relationship with the applied strain rate. This inverse correlation is attributed to the extended duration afforded by low strain rates, allowing for the development of microcracks which consequently influence the brittleness of the bone. Consequently, our research aims to combine high strain rates with low strain rates, or rather, a pre-load followed by a high-speed impact, to devise an efficient approach to induce bone fractures.

D. Materialization

1) Material

Following the conceptual design and Finite Element Analysis (FEA), the component units for each sub-system and sub-sub-system have been identified. The basis structural framework is constructed using aluminum profiles, complemented by connection components provided by Item System B.V., including 17 three-meter aluminum profiles, angle connection brackets, hinges, and T-nuts. For specific structural elements such as the roof, base, crossbeam, vertical guide, and impactor,

Figure 19: Cut aluminium profile in different length

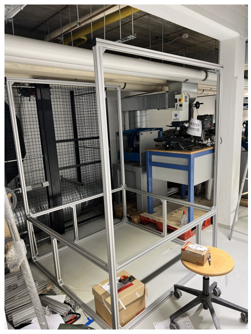

Figure 20: Frame assembly

various materials have been employed through metalworking processes. These materials include S355J2+ N structural steel, AISI 304 stainless steel, and AW-6082-T6 aluminum, all of which are sourced from CM Staal. The plastic bearing utilized for pot fixation has been sourced from BBS, while the linear ball bearings are supplied by Twenty4bearings. The electromagnet component originates from AKZYTUE, and the compression springs are procured from Amatec. Additionally, the polycarbonate plate is obtained from kunststofplatenshop, and the rubber sheet is sourced from RS Pro. Lastly, the rope used in the system is supplied by Bol.

2) Materialization of experimental apparatus

Number	Length	Usage
4	2000 mm	Vertical frame support
12	1420 mm	Base, side beam structure
7	1500 mm	Roof, motor support frame
6	300 mm	Fixation crossbeam support
2	400 mm	Fixation crossbeam support
4	1440 mm	Fixation crossbeam support

Table VIII: Aluminum profile cut

Framework assembly Aluminium profile contributes the main frame. The profile is cut in length by chainsaw. Then connected by angle connection bracket. The framework consists of 35 aluminum profile and details shown in table VIII.

Figure 21: Lathe-turning on impactor hammer using 100mm X 100mm x 30mm structural steel. Aiming to get hammer geometry: 70 mm diameter cylinder

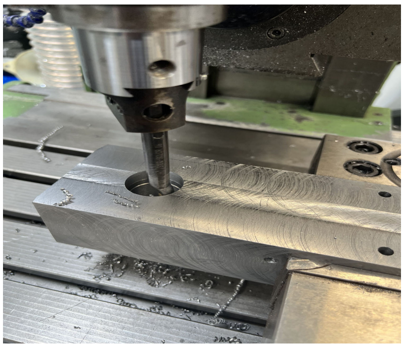

Figure 22: Fly cutter on impactor beam 400mm X 80mm X 60mm. Aiming to mill a 40 mm diameter hole with tolerance H9.

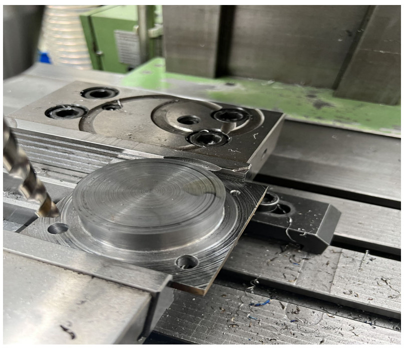

Figure 23: Milling machine with drill on impactor hammer. The drill hole diameter is 8.3 mm used for M8 bolt

Figure 24: Face mill cutter on impactor beam 400mm X 80mm X 60mm. Aiming to produce flat surface

Figure 25: End mill cutter on base plate fixation. Aiming to produce a flat

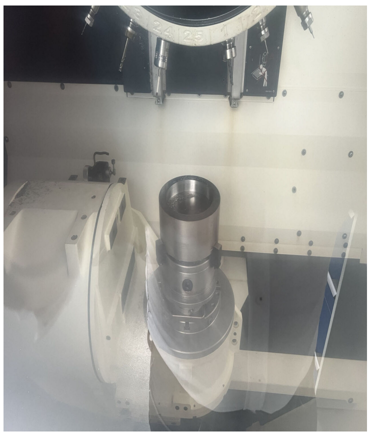

Figure 26: computer numerical control cut on pot with outside diameter 170 mm and inner diameter 130mm

Metal working: Metal S355, 304L, and 6082-T6 are processed by chainsaw, lathe and milling machine. The metal is reshaped by chainsaw to get decided size if needed. The lathe is highly efficient for producing cylindrical shapes quickly and accurately while milling machine is versatile and capable of producing a wide range of complex shapes and features. Turning and facing can remove material from a rotating parts, shown in Figure 21. Fly mill cutter mill as a inner circle and can flexibly adjust the milling diameter, but need pre hole, as shown in Figure 22. Drilling can be executed on both lathe and milling machine that can process a straight hole in the product, the difference is that sample is rotating on the lathe while drill is rotating on the milling machine, see Figure 23. Face mill cutter can remove the surface layer precisely, especially for rust removal. End mill cutter can be used for create internal slot and holes, shown in Figure 25. The computer numerical control milling is highly automated and precise in cutting and includes built-in measurement and inspection features to ensure the produced parts meet the specified tolerances and quality standards.

Bearing fit: The linear ball bearing and the Teclite plastic bearing employ a press-fit assembly method in accordance with the ISO tolerance standards for holes, specifically H9, and shafts, particularly h9 as per ISO 286-2. The linear ball bearing has an inner diameter of 30 mm, an outer diameter of 40 mm, and a length of 50 mm. The shaft, made of stainless steel, measures 1900 mm in length and has a diameter of 30 mm, adhering to the h9 surface tolerance specification. The housing holes, which accommodate the linear ball bearing, are machined on the impactor and possess diameters of 40.010 mm and 40.005 mm, respectively. On the other hand, the housing hole designed for the Teclite plastic bearing has a specified diameter of 185 mm with a tolerance of ± 0.3 mm.

IV. Result

A. Prototype

Materialization: During the actual build process, some components were improved to be suitable for the actual situation. The sub-system components are made by metalworking, including impactor hammer, impactor weight beam, base plate, 4 different unit of specimen support, guide base, spring base plate, spring core, clamp connection, and fixation beam from left to right shown in Figure 27.

The impactor hammer was crafted from S355+J structural steel and featured a square base measuring 100 mm by 100 mm, with an 80 mm diameter cylindrical extension. This component underwent a manufacturing process involving lathe turning and subsequent milling machine drilling. Similarly, the impactor weight beam was constructed from S355+J steel due to its favorable magnetization properties. To prepare the crossbeam, a face mill cutter was initially employed to remove surface rust. Subsequently, precision holes with a tolerance level of H9 were created using drilling and a fly cutter. The base plate, with dimensions of 400 mm by 400 mm by 20 mm, was fabricated from AW-6082-T6 aluminum through a drilling process. The specimen support comprised four distinct units capable of adjusting the support height by incorporating connection units. These units were fashioned from AW-6082-T6 aluminum cylinders, featuring diameters of 70 mm and 50 mm, and underwent lathe turning, facing, and drilling procedures. For the guide base, an AW-6082-T6 aluminum cylinder with a 70 mm diameter was selected and drilled with a center of 30.250 mm to accommodate the vertical guide. The guide itself could be secured in place using an inner flat end screw on the side of the base. The spring base was crafted from an AW-6082-T6 aluminum plate, featuring four large holes. Two of these holes were used in conjunction with the guide base to secure the guide, while the other two were fitted with linear ball bearings (KH3050) to facilitate the movement of the spring core. The spring core, a cylindrical component made of AW-6082-T6 aluminum, was created through lathe turning and drilling processes. To establish a connection between the electromagnet and motor cable, a clamp connection made of S235 structural steel was designed by face mill cuting and drilling. Lastly, the fixation beam was constructed from AW-6082-T6 aluminum and was meticulously processed using a CNC milling machine by DEMO.

Assembly The assembly procedure was conducted within the premises of the IWS workshop, shown in Figure 28. The apparatus was securely positioned on a base featuring a rubber layer. The aluminum profiles, specific to various sections, were interconnected using angle brackets. To firmly place the crossbeam, an inner support system was

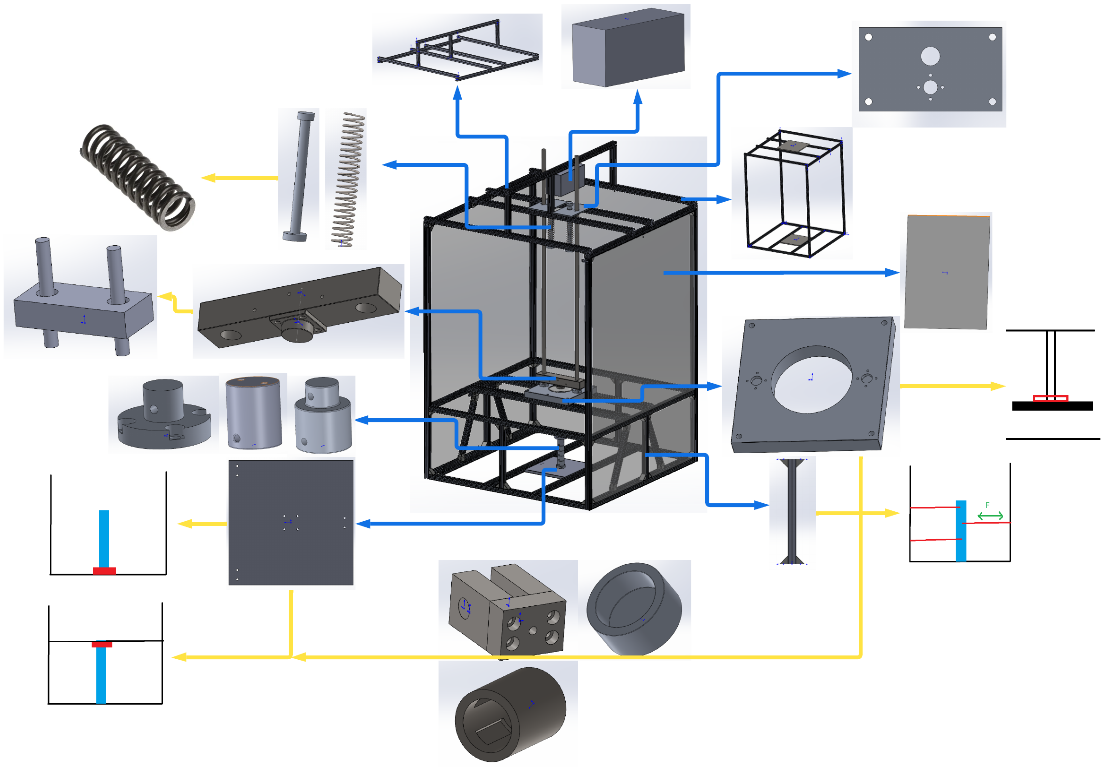

Figure 27: Processed components

employed, consisting of a bar mechanism crafted from six 300mm profiles affixed with heavy-duty hinges. Vertical guides were implemented, passing through the beam, impactor, and spring base that allow free moving of the impactor. In order to enhance the door's stability, an additional frame was introduced. To prevent the entanglement of electromagnet wires, a small pulley was integrated. Furthermore, an extra aluminum bar was installed above the roof to augment overall stability.

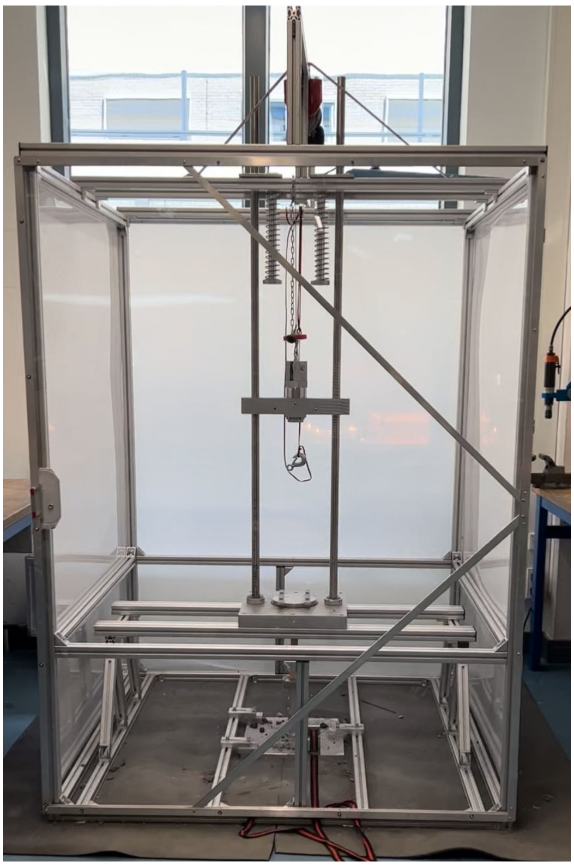

Figure 28: Prototype

B. Testing

This chapter introduce fracture simulation protocol and weight drop test.

1) Protocol

Prior to initiating a weight drop test, it is imperative to adhere to established protocols, consisting of a comprehensive set of rules, procedures, and guidelines meticulously designed to prioritize the safety and well-being of all individuals involved. The procedure is shown in Figure 29. The fracture simulation procedure inherently entails the release of a substantial impact energy, thereby posing a considerable potential risk. Consequently, it is crucial to commence with an introductory overview of the fracture simulation process, focusing on the identification of potential hazards and a meticulous assessment of the associated risk levels. Following this introductory phase, meticulous preparation of the test specimens becomes a fundamental requisite. Depending on the cadaveric region and the specific fracture type under investigation, it may necessitate a dissection of the cadaver to expose a minimum bare bone section of at least 60 millimeters, which will serve as the connection point. For the simulation materials, both bone and humongous components should be meticulously molded to match the desired length and shape specifications. The preparation process entails the mixing of cement powder with water, maintaining a specified proportion of 4 kilograms of cement powder to 500 milliliters of water. Practically, water is added to the cement powder until the mixture reaches a solid state, with adjustments made to the water quantity based on the required preparation time. Subsequently, a minimum waiting period of 15 minutes is observed to ensure the fixation of the specimen within the cement pot, with thorough scrutiny of the connection between the cement and the specimen. Four key components can be adjusted to ensure the safety of the setup: the base support, base, side beam, and rope connection, which can be manipulated using a 5-6 millimeter hexagon screwdriver. Alterations to these components afford the capability to regulate the maximum falling height, reposition the base plate, and adjust the traction direction and quantity. Once the setup is configured with the correct parameters, it is imperative for investigators to maintain a distance of at least 3 meters from the apparatus and remotely initiate the release of the impactor. Ultimately, upon the completion of the test, the fractured bone specimen is subjected to a CT-scan, followed by further analysis conducted by a qualified surgeon.

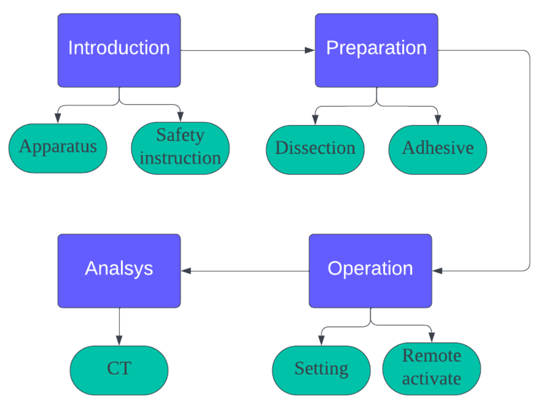

Figure 29: Protocol flowchat

2) Drop test

In this research investigation, three distinct categories of specimens had been incorporated. These categories encompass human specimens, comprising anatomical elements such as the forearm, tibia, and hip. Secondly, simulation bones possessing bionic geometrical properties and physical attributes akin to those found in human bones were utilized. Thirdly, humongous materials, represented by concrete pillars crafted through the molding process utilizing Polyvinyl Chloride (PVC) tubes and cement, were also included in this study shown in Table IX.

First saw bone test: In the initial weight drop experiment, a humerus saw bone was used. The bone was connected with fitting by cement. The bone was securely affixed using cement to ensure a stable connection. During the initial phase of impact testing, an energy input of 10 Joules was administered, resulting in the bone's structural integrity remaining uncompromised. However, during a subsequent test, where the energy level was elevated to 30 Joules, a sudden fracture of the saw bone occurred, resulting in the bone splitting into two distinct pieces, as illustrated in Figure 30. Notably, no other significant observations or alterations in the bone's behavior were documented within the energy range spanning from 10 to 30 Joules.

Specimen	Fixation	Height	Energy	State
Saw bone 1	Top fixation	0.071 m	10 Joules	intact
Saw bone 1	Top fixation	0.214 m	30 Joules	fractured and broken
Cement bar 1	Top fixation	-	-	broken after preparation
Cement bar 2	Top fixation	-	-	broken after preparation
Cement bar 3	Top fixation	-	-	broken after preparation
Cement bar 4	Top fixation	-	-	broken due to pot weight
Saw bone 2	Top fixation	0.036 m	5 Joules	intact
Saw bone 2	Top fixation	0.071 m	10 Joules	intact
Saw bone 2	Top fixation	0.0143 m	20 Joules	intact
Saw bone 2	Top fixation	0.214 m	30 Joules	intact
Saw bone 2	Top fixation	0.286 m	40 Joules	intact
Saw bone 2	Top fixation	0.357 m	50 Joules	intact
Saw bone 2	Fixation & traction	0.036 m	50 Joules	intact
Reinforced broom	Top fixation	0.036 m	5 Joules	intact
Reinforced broom	Top fixation	0.071 m	10 Joules	intact
Reinforced broom	Top fixation	0.143 m	20 Joules	intact
Reinforced broom	Top fixation	0.286 m	40 Joules	intact
Reinforced broom	Top fixation	0.571	80 Joules	intact
Reinforced broom	Fixation & traction	0.571 m	80 Joules	intact
Reinforced broom	Top fixation	1.072 m	150 Joules	intact
Reinforced broom	Top fixation	1.30 m	230 Joules	specimen slide out

Table IX: Drop test

Figure 30: Saw bone 1

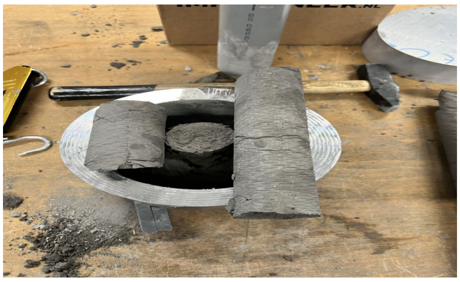

Figure 31: Cement bar broken

Figure 32: Rope system

Figure 33: Saw bone 2

Homogeneous materials test: In the following experimental configuration, cement bars served as the designated test specimens. These bars were formed by encapsulating cement material within Polyvinyl Chloride (PVC) pipes and then wrapping them with paper to achieve the desired shape. It is noteworthy that the substantial water content incorporated into the cement mixture hindered the drying process of the bars. As a result, the preparation of the cement specimens proved to be time-consuming and characterized by inefficiency. See Figure 31.

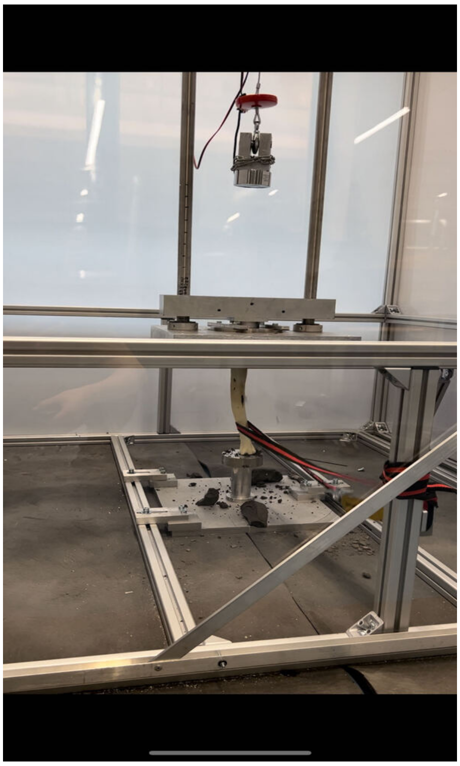

Figure 34: Rope loose

Figure 35: broom

Second saw bone The second simulation involved the use of a tibia saw bone, which was subjected to the same treatment as saw bone 1, illustrated in Figure 33. Energy inputs were applied in the range of 5 to 50 Joules, with the addition of traction force to induce a preliminary moment on the specimen. It is important to note that impact energies exceeding 50 Joules were not administered due to concerns regarding the fragile connection between the saw bone, cement, and pot. The cement, which had not fully dried, was observed to lose its adhesive properties, leading to a detachment of the cement connection during the 50 Joules test. Besides, the tibia saw bone has significant bending deformation which leads to loose of the rope during the test.

Extreme test The broom used in the experiment was constructed with reinforced wood, specifically designed for safety and stability testing under extreme power output conditions. To increase the impact energy, the height from which the impactor was released was gradually raised, ranging from 5 to 150 Joules. Notably, at a height of 1.08 meters, the impactor initiated contact with the spring system, subsequently reaching its maximum potential energy at a height of 1.3 meters. This energy level, calculated using equation 16, amounted to 230 Joules. It is important to emphasize that following the rigorous testing, the broom remained structurally intact, and the entire experimental system exhibited stability without sustaining any damage.

V. Discussion

A. Prototype

Materialization The fabrication of the fracture device designed for forearm fracture testing has been successfully completed. It's important to note that the manufacturing process for each component of this device involved variations in materials, sizes, cutting methods, and cutting speeds. These variations were dictated by the unique properties of the materials used. Stainless steel AISI 304L is harder compared to structural steel S355 and aluminum AW-6082-T6. To produce components that are in same size, it was necessary to reduce the rotation speed of the cutter when working with stainless steel AISI 304L and structural steel S355. Furthermore, as the size of the processed part increased, it became imperative to lower the cutting speed. This adjustment was made to ensure precise and consistent manufacturing across components of varying materials and sizes. During the cutting process, friction generated heat in the metal, leading to changes in volume. To maintain precision, the use of a cooling liquid was essential. This cooling process helped mitigate the effects of thermal expansion and contraction, ensuring that the final dimensions of the components were accurate and it is necessary to do the assembly after cooling. Additionally, it's important to consider that the initial material used may have certain tolerances, which can result in surfaces that are not perfectly flat or parallel. To rectify this, necessary adjustments were made to ensure that the material's surfaces were appropriately aligned and flat before proceeding with the manufacturing process. This step was crucial to guarantee the overall quality and reliability of the fracture device.

Apparatus The final configuration of the apparatus measured 1.5 meters in length, 1.5 meters in width, and 2.34 meters in height, with a total cost of 4749 euros. The apparatus was finally assembled in Amsterdam Skill Centre.In terms of stability, it capably supports a vertical load, maintaining its equilibrium with ease. However, it exhibits some vulnerability when subjected to horizontal forces, resulting in a noticeable frame oscillation. A noteworthy concern arises with the compression spring within the core of the apparatus. At full compression, the spring fails to reach complete compression, causing slight bending. This subtlety in the spring's behavior demands close attention, as it influence experimental maximum impact energy output.The rope system is an integral component of the apparatus, linked to a dynamometer for force measurement. However, its operational complexity becomes apparent due to the separation of these two critical elements. During testing, specimens may undergo bending, leading to potential detachment of the rope connection from the cadaver, a situation that merits careful consideration. The adjustable fixation crossbeam has been incorporated into the design with bar mechanism. This adaptive feature ensures that the apparatus can accommodate varying specimen lengths effectively. The motor control system used to adjust the height of the impactor exhibits some limitations in terms of precision. The rotation of the motor cannot be precisely controlled, which may impact the accuracy of height adjustments.

B. *Experiment*

Simulation bone test: The weight drop test yielded intriguing findings when applied to saw bones of distinct bone types and varying lengths. Notably, the maximum impact energy that these specimens could withstand varied significantly. In the case of humerus saw bones, there was a pronounced discrepancy in thickness among the specimens. Conversely, tibia saw bones exhibited a more consistent thickness profile. Therefore, humerus saw bones succumb to fractures under the influence of a 30 Joules impact, while the tibia saw bones demonstrate remarkable resilience, enduring impacts exceeding 50 Joules. It's worth highlighting that these experiments were conducted without the presence of human tissue, but still allowing for a comparison with Wegmann's study. When evaluating the results, it becomes evident that an impact energy of 30 Joules, though seemingly modest, proved to be remarkably efficient. This is particularly noteworthy when considering that Wegmann's study reported fracture energies ranging from 64 to 184 Joules. The effectiveness of the less impact energy in this context suggests the potential for enhanced efficiency in similar experimental setups.

Homogeneous material test: Creating a concrete bar with a 30mm-diameter using a PVC tube involves the mixture of cement with an adequate amount of water to achieve the desired liquidity for pouring into the container. However, it's important to be mindful of the consequences of excess water in this process. Firstly, adding excessive water can lead to the formation of bleeding channels within the concrete during the hardening process. Bleeding refers to the migration of water to the surface of the concrete mix, resulting in the segregation of fine particles and water from the rest of the mixture. This can compromise the homogeneity of the concrete, potentially affecting its structural integrity. Secondly, an excessive water-to-cement ratio can reduce the overall strength of the concrete. The strength of concrete is influenced by the chemical reactions that occur as it cures, and an excess of water can disrupt these reactions, leading to weaker concrete. Moreover, the presence of excess water can create a weakened layer within the concrete, making it more susceptible to cracks and structural deficiencies. These cracks can compromise the durability and longevity of the concrete structure. It's crucial to carefully control the water-cement ratio when preparing concrete mixes to ensure the desired consistency without compromising the strength and quality of the final product.

Extreme test: In the fracture device strength test, a reinforced wood stick was employed, showcasing the overall stability of the system even under the most demanding energy outputs. However, a noteworthy weakness emerged in the form of the cement-based connections. These connections proved to be vulnerable to the shockwaves generated by the impact, leading to their detachment from both the fitting pot and specimen. While addressing this issue, it's essential to consider alternatives. One viable option is to utilize low-melting-point metals, such as bismuth alloys. These mExtremeaterials offer improved resistance to impact-induced disconnection due to their inherent properties. However, it's important to acknowledge that this solution comes at a higher cost, same as bone cement, which impact the project's budget considerations. Careful evaluation of cost-effectiveness and performance benefits will be essential in determining the optimal approach to address this weak point in the system.

C. *Future work*

Cadaver specimen experiment: All the experiments conducted thus far have been predicated on the utilization of simulation materials. Our forthcoming research endeavors entail inducing controlled fractures in cadaveric specimens, all while preserving the integrity of the overlying skin. In these upcoming experiments, we aim to evaluate three distinct fixation methods, either individually or in combination. Two crucial parameters will be subjected to measurement:

1. Impactor Force Analysis: The primary focus of this analysis is to discern the impactor force applied during the fracture-inducing event. This force is directly associated with the brittleness of the specimen. Additionally, we intend to ascertain the upper threshold of the force required to cause a fracture. By doing so, we can gain insights into the material's susceptibility to fracture under specific loading conditions.
2. Microcrack Quantification via CT-Scan: The second key measurement pertains to the quantification of microcracks within the cadaveric specimen. These microcracks will be assessed using advanced imaging techniques, particularly computed tomography (CT) scans. The objective is to investigate whether the number of microcracks increases when the cadaveric specimen is subjected to traction forces. This evaluation will offer valuable insights into the specimen's response to different loading conditions and fixation methods.

The transition from simulation materials to cadaveric specimens represents a significant advancement in our experimental approach, as it aligns more closely with real-world scenarios and provides a more comprehensive understanding of fracture behavior.

Impact force estimation: In the conducted experiment, we didn't use stress or strain sensors to quantify parameters such as force, vibrations, and impulse time. This decision was primarily influenced by time constraints , budget, and the anticipated workload and intricacy associated with integrating a sensor system. Based on current study, the best way is the direct approach by measuring force using force or stress sensors. This choice was motivated by the recognition that even calculations based on force-time and force-distance relationships, in equations 19 and 20, inherently possess a degree of imprecision. It is important to acknowledge that measurements inherently contain some level of error, and this error can accumulate when propagated through calculations and subsequent measurements. Therefore, we determined that employing force sensors directly would provide a more accurate and reliable means of capturing the force-related data within the scope of our experiment. This approach minimizes the potential for error accumulation, ensuring the integrity of our results.

VI. Conclusion

A fracture device is constructed for cadaver bone fracture simulation in this master thesis. The controllable fracture device boasts a sturdy and stable construction while operating as a versatile modular system. This design flexibility opens the door to substantial potential for enhancements and further experimentation. One critical area warranting attention is the precision of motor control, which presently exhibits instability in regulating motor rotation. Addressing this concern is paramount to ensure the device's reliability for accurate and precise experimental setups. The addition of a small-range height adjuster holds promise in refining control mechanisms, granting finer adjustments for optimal device performance. Additionally, the device could greatly benefit from the incorporation of a force measurement system and an upgraded connection unit for the rope system. These improvements are poised to significantly enhance the efficiency of rope connections, ultimately resulting in more dependable and consistent outcomes during experimentation.

There exists another intriguing avenue for development – the creation of a compact, movable device tailored specifically for smaller cadaver regions. This innovation would cater to the unique needs of such specimen. It relies on implementing a robust tiny power system, capable of delivering substantial impact power, may necessitate a high-power-volume system, potentially inducing spring discs to achieve the desired impact force.

In future experiments, the focus will be on testing three different fixation methods individually and in combination. The primary objectives will be to measure the impact force during fracture and quantify the number of microcracks in the bone. These parameters will serve as key references for studying bone characteristics and evaluating the effectiveness of different fixation techniques.

References

[1] A. S. Siddiquey, S. S. Husain, and S. Z. H. Laila, "History of anatomy," *Bangladesh Journal of Anatomy*, vol. 7, no. 1, pp. 1–3, 2009.

[2] L. O. Dissabandara, S. N. Nirthanan, T. K. Khoo, and R. Tedman, "Role of cadaveric dissections in modern medical curricula: a study on student perceptions," *Anatomy & cell biology*, vol. 48, no. 3, pp. 205–212, 2015.

[3] J. Cochrane, "Precepts of infection prevention and control," *Essential Skills Clusters for Nurses: Theory for Practice. Chichester: Wiley-Blackwell*, pp. 143–61, 2009.

[4] C. A. Berezowsky, R. P. Hoyos, P. B. Lourenco, *et al.*, "Experience using immersive virtual reality simulation during an ao trauma regional course in latin america," *Journal of Musculoskeletal Surgery and Research*, vol. 6, no. 4, pp. 278–282, 2022.

[5] W. Clifton, A. Damon, E. Nottmeier, and M. Pichelmann, "The importance of teaching clinical anatomy in surgical skills education: Spare the patient, use a sim!," *Clinical Anatomy*, vol. 33, no. 1, pp. 124–127, 2020.

[6] A. Beaven, D. Griffin, and H. James, "Highly realistic cadaveric trauma simulation of the multiply injured battlefield casualty: an international, multidisciplinary exercise in far-forward surgical management," *Injury*, vol. 52, no. 5, pp. 1183–1189, 2021.

[7] R. P. Blom, D. Mol, L. J. van Ruijven, G. M. Kerkhoffs, and T. H. Smit, "A single axial impact load causes articular damage that is not visible with micro-computed tomography: an ex vivo study on caprine tibiotalar joints," *Cartilage*, vol. 13, no. 2_suppl, pp. 1490S–1500S, 2021.

[8] C. Yan, H. Song, J. Pfister, T. L. Andersen, S. J. Warden, R. Bhargava, and M. E. Kersh, "Effect of fatigue loading and rest on impact strength of rat ulna," *Journal of Biomechanics*, vol. 123, p. 110449, 2021.

[9] I. T. Haider, M. Lee, R. Page, D. Smith, and W. B. Edwards, "Mechanical fatigue of whole rabbit-tibiae under combined compression-torsional loading is better explained by strained volume than peak strain magnitude," *Journal of Biomechanics*, vol. 122, p. 110434, 2021.

[10] S. M. Kerrigan, A. S. Kapatkin, T. C. Garcia, D. A. Robinson, D. S.-M. Guzman, and S. M. Stover, "Torsional and axial compressive properties of tibiotarsal bones of red-tailed hawks (buteo jamaicensis)," *American journal of veterinary research*, vol. 79, no. 4, pp. 388–396, 2018.

[11] J. C. McGinley, B. C. Hopgood, J. P. Gaughan, K. Sadeghipour, and S. H. Kozin, "Forearm and elbow injury: the influence of rotational position," *JBJS*, vol. 85, no. 12, pp. 2403–2409, 2003.

[12] N. Ott, A. Harbrecht, M. Hackl, T. Leschinger, J. Knifka, L. Müller, and K. Wegmann, "Inducing pilon fractures in human cadaveric specimens depending on the injury mechanism: a fracture simulation," *Archives of Orthopaedic and Trauma Surgery*, vol. 141, no. 5, pp. 837–844, 2021.

[13] K. Wegmann, A. Harbrecht, M. Hackl, S. Uschok, T. Leschinger, and L. P. Müller, "Inducing life-like distal radius fractures in human cadaveric specimens: a tool for enhanced surgical training," *Archives of Orthopaedic and Trauma Surgery*, vol. 140, no. 3, pp. 425–432, 2020.

[14] K. Wegmann, N. Ott, M. Hackl, T. Leschinger, S. Uschok, A. Harbrecht, J. Knifka, and L. Müller, "Simulation of life-like distal humerus and olecranon fractures in fresh frozen human cadaveric specimens," *Obere Extremität*, vol. 15, no. 2, pp. 137–141, 2020.

[15] A. Harbrecht, M. Hackl, T. Leschinger, S. Uschok, L. Müller, and K. Wegmann, "Metacarpal fractures—a method to simulate life-like fractures in human cadaveric specimens for surgical education," *Hand Surgery and Rehabilitation*, vol. 41, no. 2, pp. 214–219, 2022.

[16] A. Harbrecht, F. Endlich, M. Hackl, K. Seyboth, B. Lethaus, L. P. Müller, and K. Wegmann, "“crack under pressure”—inducing life-like mandible fractures as a potential benefit to surgical education in oral and maxillofacial surgery," *Annals of Anatomy-Anatomischer Anzeiger*, vol. 240, p. 151878,

2022.
[17] K. Wegmann, K. Engel, K. J. Burkhart, M. Ebinger, R. Holz, G.-P. Brüggemann, and L. P. Müller, “Sequence of the essex-lopresti lesion—a high-speed video documentation and kinematic analysis,” *Acta orthopaedica*, vol. 85, no. 2, pp. 177–180, 2014.
[18] “Ao foundation surgery reference,” Mar 2023.
[19] Y. Zhang and X. Xing, “Classifications of hand and wrist fractures,” in *Clinical Classification in Orthopaedics Trauma*, pp. 183–230, Springer, 2018.
[20] A. Van Boeijen, J. Daalhuizen, R. van der Schoor, and J. Zijlstra, *Delft design guide: Design strategies and methods*. 2014.
[21] M. Watson, B. Mesmer, and P. Farrington, “Engineering elegant systems: Theory of systems engineering,” 2020.
[22] S. Şengel, H. Erol, T. Yılmaz, and Ö. Anıl, “Investigation of the effects of impactor geometry on impact behavior of reinforced concrete slabs,” *Engineering Structures*, vol. 263, p. 114429, 2022.
[23] A. K. Bhat, R. Jindal, and A. M. Acharya, “The influence of ethnic differences based on upper limb anthropometry on grip and pinch strength,” *Journal of Clinical Orthopaedics and Trauma*, vol. 21, p. 101504, 2021.
[24] MITCalc, “Springs calculation.”
[25] roymech, “Disc spring design.”
[26] N. P. Mastricola and R. Singh, “Nonlinear load-deflection and stiffness characteristics of coned springs in four primary configurations,” *Mechanism and Machine Theory*, vol. 116, pp. 513–528, 2017.
[27] “Bellevillesprings,” Oct 2022.
[28] R. Metz, “Impact and drop testing with icp force sensors,” *pulse*, vol. 2, pp. 2–2, 2006.
[29] J.-Y. Rho, L. Kuhn-Spearing, and P. Zioupos, “Mechanical properties and the hierarchical structure of bone,” *Medical engineering & physics*, vol. 20, no. 2, pp. 92–102, 1998.
[30] S. H. Ralston, “Bone structure and metabolism,” *Medicine*, vol. 41, no. 10, pp. 581–585, 2013.
[31] J. F. Knott, *Fundamentals of fracture mechanics*. Gruppo Italiano Frattura, 1973.
[32] D. Vashishth, “Rising crack-growth-resistance behavior in cortical bone:: implications for toughness measurements,” *Journal of biomechanics*, vol. 37, no. 6, pp. 943–946, 2004.
[33] P. Augat and S. Schorlemmer, “The role of cortical bone and its microstructure in bone strength,” *Age and ageing*, vol. 35, no. suppl_2, pp. ii27–ii31, 2006.
[34] F. A. Sabet, A. Raeisi Najafi, E. Hamed, and I. Jasiuk, “Modelling of bone fracture and strength at different length scales: a review,” *Interface focus*, vol. 6, no. 1, p. 20150055, 2016.
[35] P. Zioupos, U. Hansen, and J. D. Currey, “Microcracking damage and the fracture process in relation to strain rate in human cortical bone tensile failure,” *Journal of biomechanics*, vol. 41, no. 14, pp. 2932–2939, 2008.

]

Appendix

A. FEA result

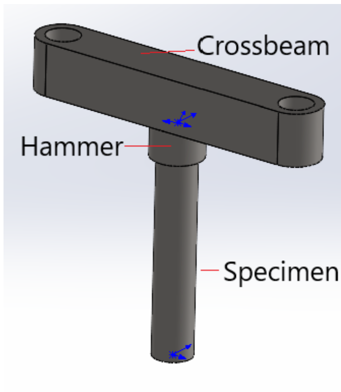

Figure 36: Simplified impact test model

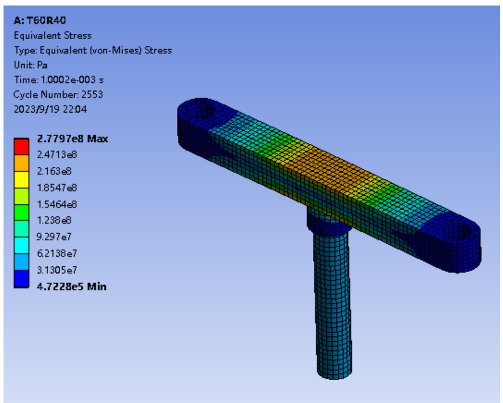

Figure 37: Stress distribution of crossbeam with length 680mm, width 80mm, and thickness 60mm

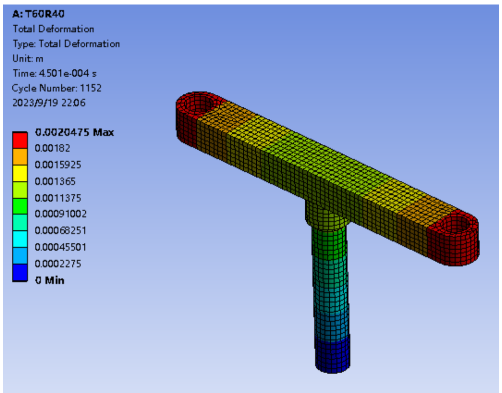

Figure 38: Deformation distribution of crossbeam with length 680mm, width 80mm, and thickness 60mm

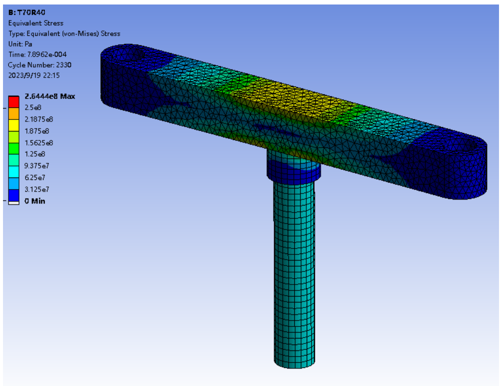

Figure 39: Stress distribution of crossbeam with length 680mm, width 80mm, and thickness 70mm

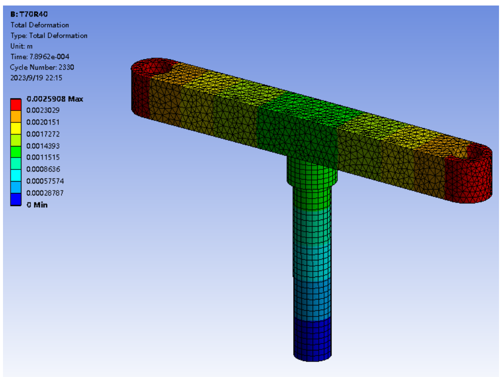

Figure 40: Deformation distribution of crossbeam with length 680mm, width 80mm, and thickness 70mm

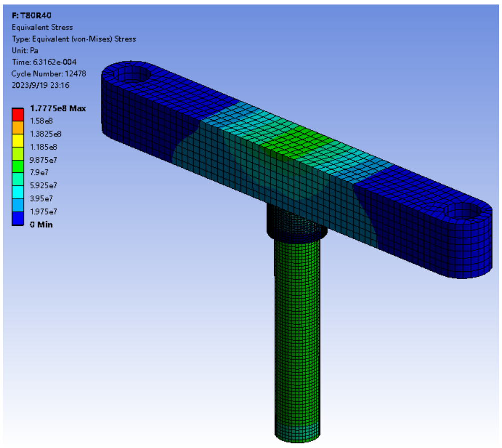

Figure 41: Stress distribution of crossbeam with length 680mm, width 80mm, and thickness 80mm

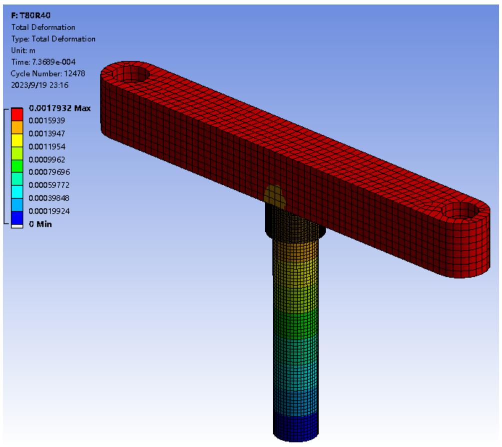

Figure 42: Deformation distribution of crossbeam with length 680mm, width 80mm, and thickness 80mm

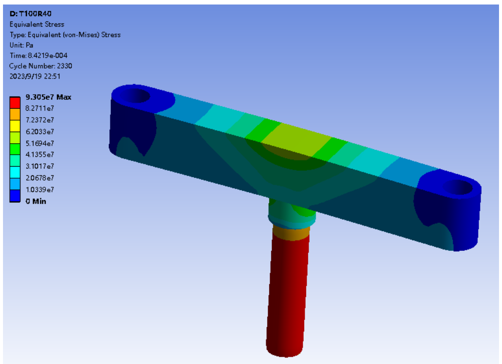

Figure 43: Stress distribution of crossbeam with length 680mm, width 80mm, and thickness 100mm

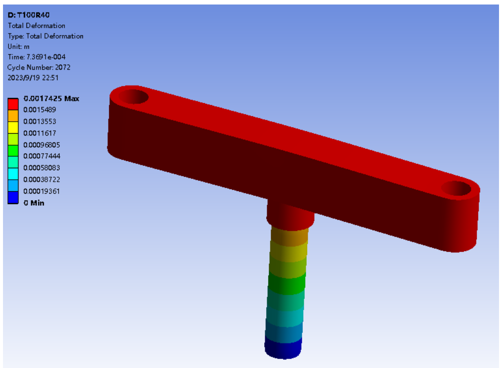

Figure 44: Deformation distribution of crossbeam with length 680mm, width 80mm, and thickness 100mm

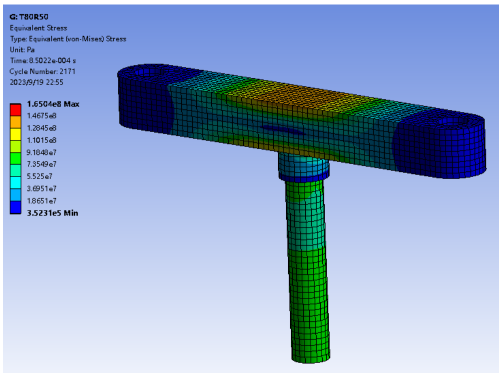

Figure 45: Stress distribution of crossbeam with length 680mm, width 100mm, and thickness 80mm

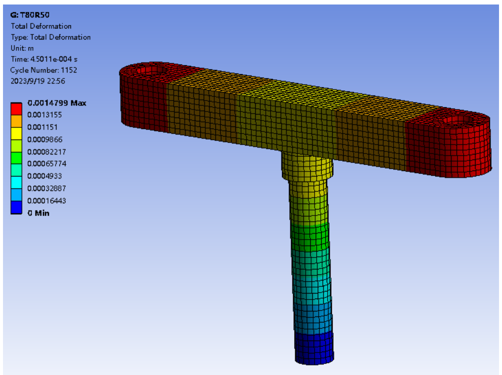

Figure 46: Deformation distribution of crossbeam with length 680mm, width 100mm, and thickness 80mm

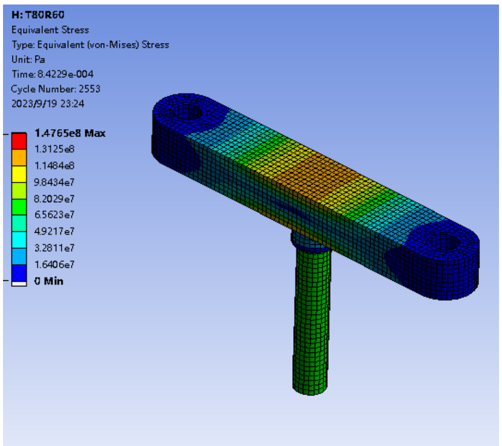

Figure 47: Stress distribution of crossbeam with length 680mm, width 120mm, and thickness 80mm

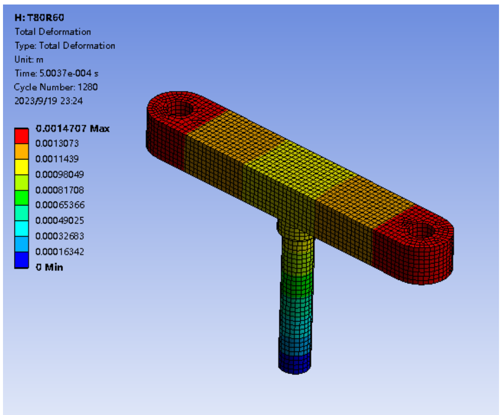

Figure 48: Deformation distribution of crossbeam with length 680mm, width 120mm, and thickness 80mm

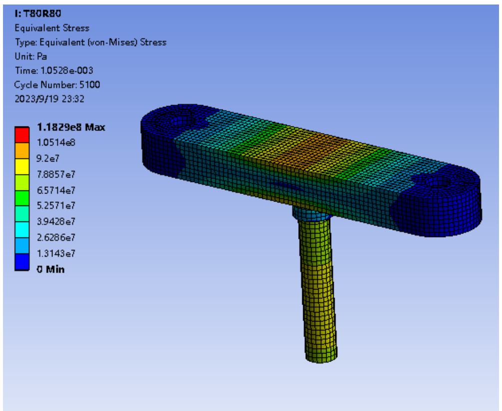

Figure 49: Stress distribution of crossbeam with length 680mm, width 160mm, and thickness 80mm

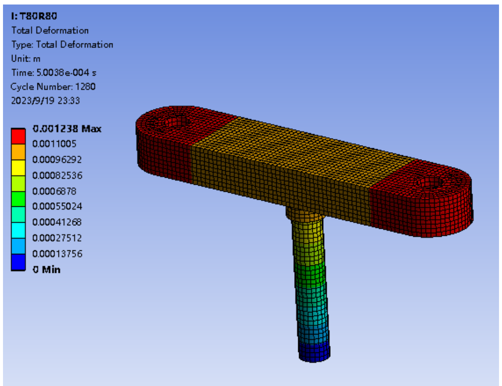

Figure 50: Deformation distribution of crossbeam with length 680mm, width 160mm, and thickness 80mm

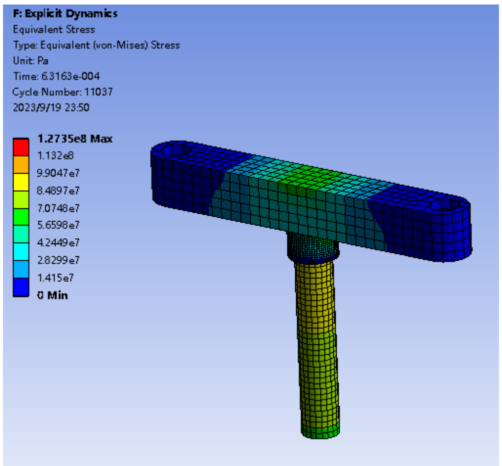

Figure 51: Stress distribution of crossbeam with length 580mm, width 80mm, and thickness 80mm

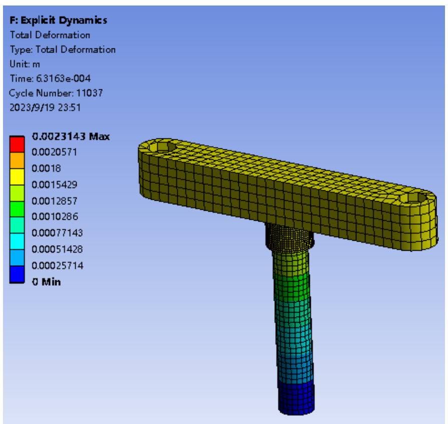

Figure 52: Deformation distribution of crossbeam with length 580mm, width 80mm, and thickness 80mm

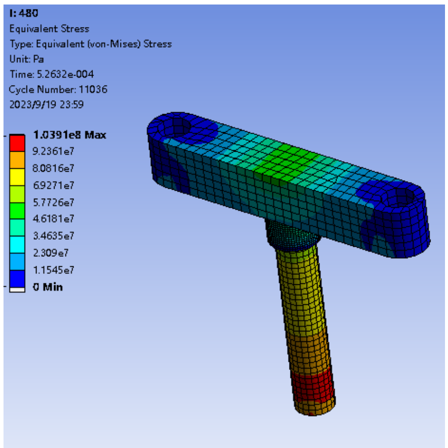

Figure 53: Stress distribution of crossbeam with length 480mm, width 80mm, and thickness 80mm

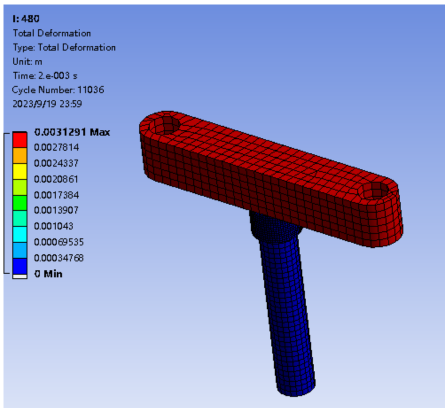

Figure 54: Deformation distribution of crossbeam with length 480mm, width 80mm, and thickness 80mm

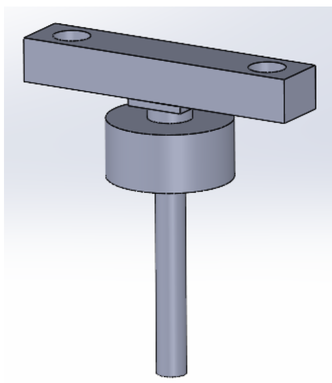

Figure 55: Improved model test

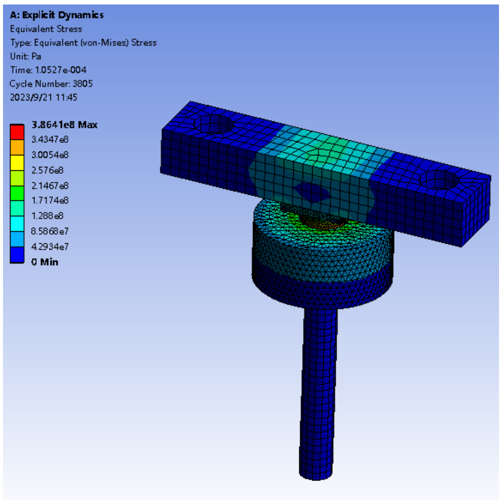

Figure 56: Deformation distribution of crossbeam with length 480mm, width 80mm, and thickness 60mm

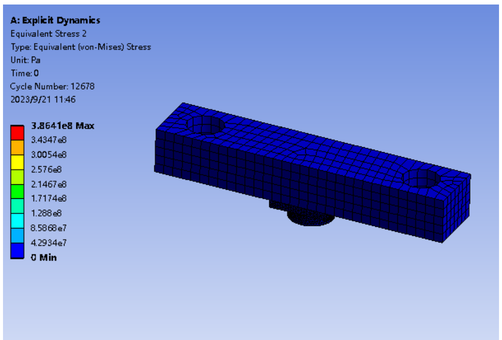

Figure 57: Stress distribution of crossbeam with length 400mm, width 80mm, and thickness 60mm

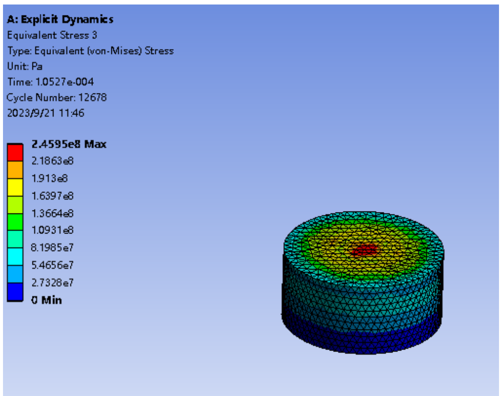

Figure 58: Stress distribution of Pot, diameter 170mm, length 80mm

B. Product data

Aluminium profile and connection component: the product are provided by Item System B.V., including

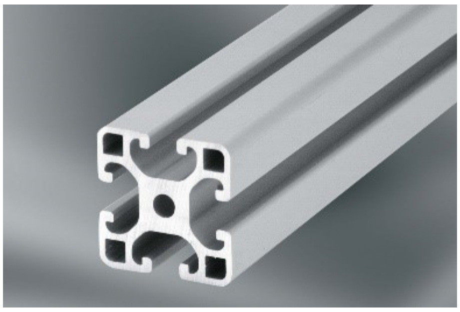

Figure 59: Aluminium profile 40 X 40, product number: 0002633

Figure 60: Bracket V 8 40 mm Z, product number: 0048628

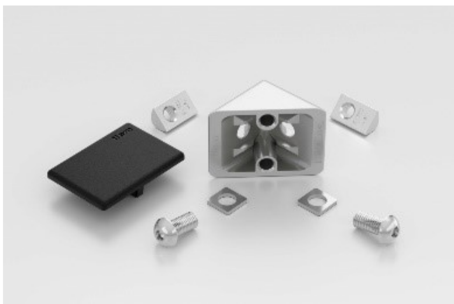

Figure 61: Bracket Set 8 40 X 40 mm, product number: 0041115

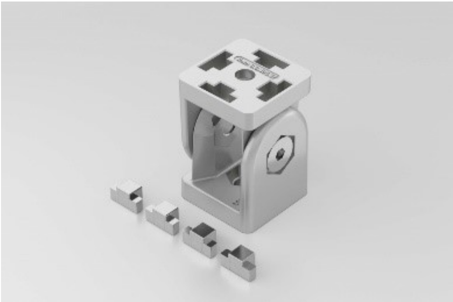

Figure 62: Hinge 8 40x40 mm, heavy-duty, product number: 0026531

Figure 63: T-Slot Nut V 8 St M8, bright zinc-plated, product number: 0048048

Figure 64: Cap 8 40x40, black, product number: 0002601

Figure 65: Hinge St, white aluminium, product number: 0064947

Figure 66: Ball Latch 8 PA, product number: 0038820

Figure 67: Handle Pi 80 M5 PA, grey, black, product number: 0067907

Other components and information:

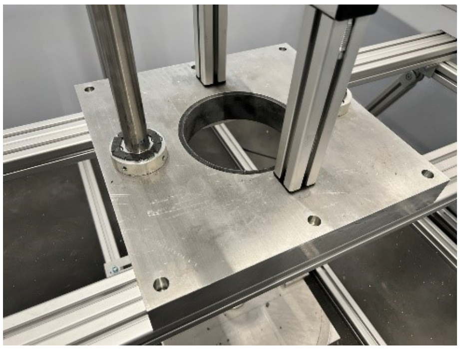

Figure 68: Top fixation beam, 400 mm X 400 mm X 50 mm AW-6082-T6

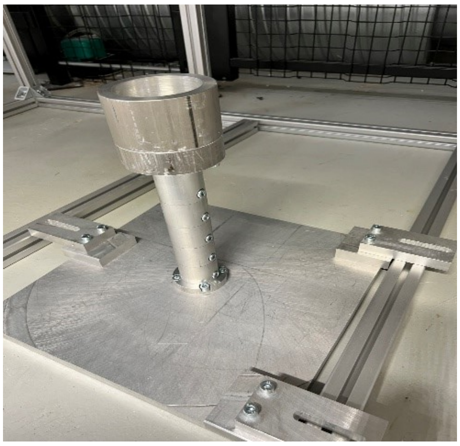

Figure 69: Base, 400 mm X 400 mm X 20 mm AW-6082-T6

Figure 70: Support, Five support units 60 mm Length, 50 mm diameter AW-6082-T6

Figure 71: Vertical guide, AISI 304, 1900 mm length, 30 mm diameter

Figure 72: Linear ball bearing, KH3050 NTN 30 (inner)-40 (outside) - 50 (length) mm

Figure 73: Plastic bearing,Teclite 170 (inner)-185 (outside) - 50 (length) mm

Figure 74: Cement pot,AISI 304, 170 (Diameter) x 80 mm

Figure 75: Motor, HBM Electric Hoist With Wireless Remote Control

Figure 76: Electromagnet, DC 24V, 0.58A, 1200N 220LB/100Kg Electric Lifting Magnet Solenoid Suction Electromagnet Holding , 80 x 38mm

Figure 77: Power supply, DC24V 0.58 A

Figure 78: Remote control socket

Figure 79: Polycarbonate plate,clear 2 mm 2000 x 1500 mm

Figure 80: RS PRO Black Rubber Sheet, 1m x 2m x 6mm

Figure 81: Benson Lashing straps - Lashing strap - Black - 2 parts - 2.5 meters - Binding belts

Figure 82: Linear compression spring,Amatec Product number: A-RDF2684

C. Impactor safety and work state

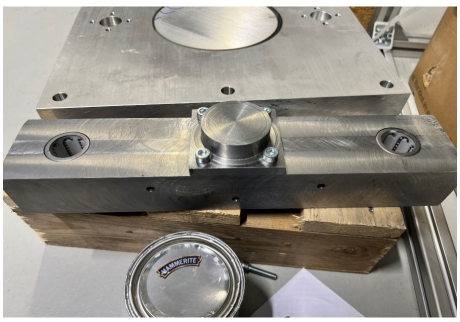

Figure 83: Weight crossbeam: S355J2+N, 400 mm X 80 mm X 60 mm; Impact hammer: S355J2+N, 80 mm X 80 mm X 30 mm Connected with 4 M8 bolts. Total weight:14.27 kg

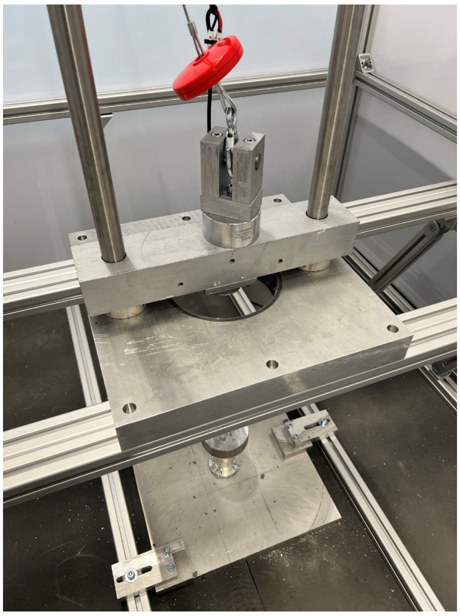

Figure 84: The impactor rest on the crossbeam and personnel is allowed to enter, closely observe and operate.

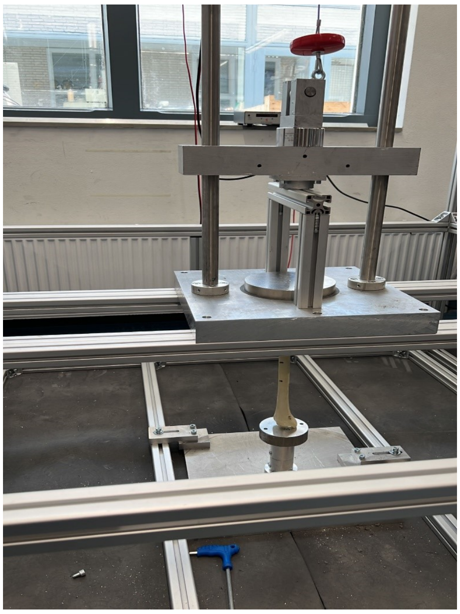

Figure 85: The impactor is rested on an aluminium profile support. The pot can be inserted from bottom.

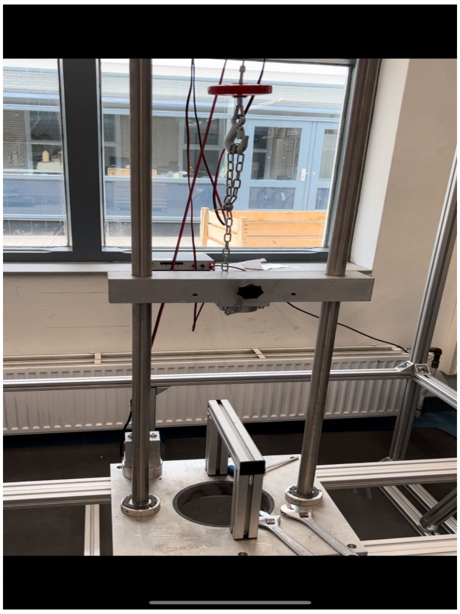

Figure 86: A lock chain with M8 bolt is connected to the motor hook while a M8 bolt is screwed into the middle-threaded hole of the impactor (both sides are the same). The impactor can be lifted up to give enough space for operation under power state and can be locked at desired heigh without the spring system under power off state.

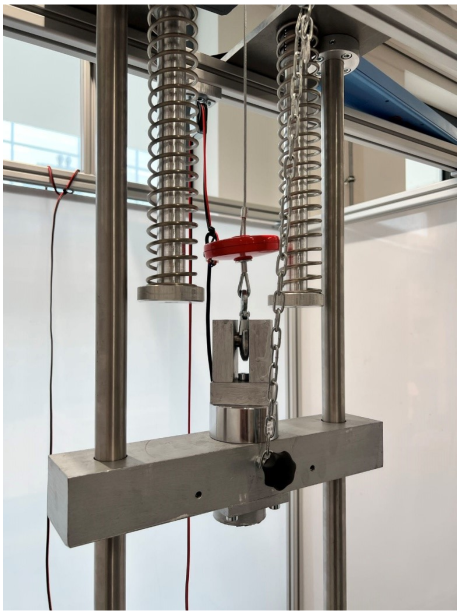

Figure 87: The lock chain, which can withstand 100 kg force, is connected to the top frame. The impactor is clamped by electromagnet and move to a certain height. Connecting the lock chain and impactor by M8 bolt.

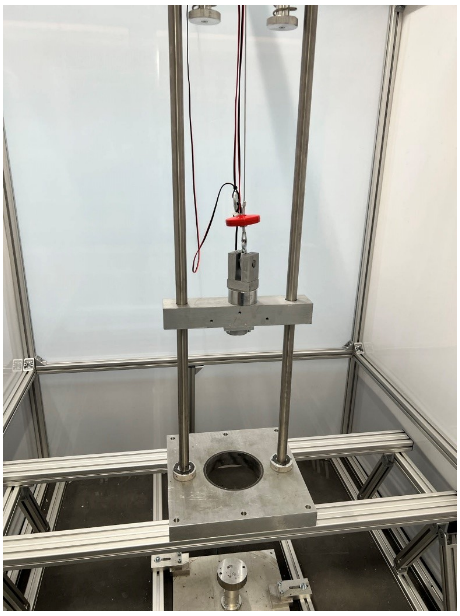

Figure 88: The electromagnet is activated by 24 V and 0.58 A power supply, which can provide 120N force to clamp the impactor. The impactor can move up and down. Once the power is off, the impactor will be in free fall and transfer gravitational potential energy into kinetic energy and later impact energy.

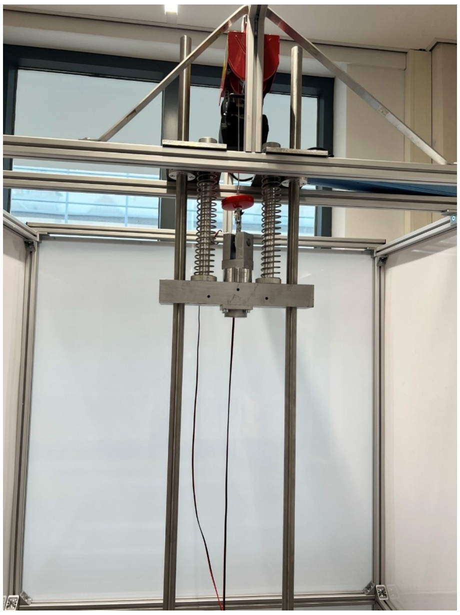

Figure 89: To increase total potential energy, the spring system can be used. Each spring can provide maximum 200 N force and 25 J elastic potential energy.

D. *Controller*

Figure 90: Controller

The above figure shows two controllers. Left one is the controller for the power source. Its button on left side is on while right side is off. Channel 1 controls the motor power and channel 2 controls the power supply for the electromagnet. Channel 3 is not used and channel 4 controls both. The motor controller can start working while the power is on (channel 1 is on), knob to "on" state, and "START" button is clicked.